Power System Parameter Estimation for Enhanced Grid Stability Assessment in Systems with Renewable Energy Sources

Andreas J. Schmitt

Dissertation submitted to the Faculty of the
Virginia Polytechnic Institute and State University
in partial fulfillment of the requirements for the degree of

Doctor of Philosophy
in
Electrical and Computer Engineering

Jaime De La ReeLopez, Chair
Virgilio Centeno, Co-Chair
Vassilis Kekatos
Werner Kohler
Amos Abbott
Kevin D. Jones

April 24, 2018
Blacksburg, Virginia

Keywords: Power System Topology Estimation, Low Observability State Estimation,
System Identification, Inertia Estimation, Power System Stability

Power System Parameter Estimation for Enhanced Grid Stability Assessment in Systems with Renewable Energy Sources

Andreas J. Schmitt

(ABSTRACT)

The modern day power grid is a highly complex system; as such, maintaining stable operations of the grid relies on many factors. Additionally, the increased usage of renewable energy sources significantly complicates matters. Attempts to assess the current stability of the grid make use of several key parameters, however obtaining these parameters to make an assessment has its own challenges. Due to the limited number of measurements and the unavailability of information, it is often difficult to accurately know the current value of these parameters needed for stability assessment. This work attempts to estimate three of these parameters: the Inertia, Topology, and Voltage Phasors. Without these parameters, it is no longer possible to determine the current stability of the grid. Through the use of machine learning, empirical studies, and mathematical optimization it is possible to estimate these three parameters when previously this was not the case. These three methodologies perform estimations through measurement-based approaches. This allows for the obtaining of these parameters without required system knowledge, while improving results when systems information is known.

Power System Parameter Estimation for Enhanced Grid Stability Assessment in Systems with Renewable Energy Sources

Andreas J. Schmitt

(GENERAL AUDIENCE ABSTRACT)

Stable grid operations means that electricity is supplied to all customers at any given time regardless of changes in the system. As the power grid grows and develops, the number of ways in which a grid can lose stability also grows. As a result, the metrics that are used to determine if a grid is stable at any given time have grown increasingly complex and rely on significantly more amounts of information. This information required in order to obtain the metrics which determine grid stability often has key limitations in when and how it can be obtained. The work presented details several methods for obtaining this information in situations were it was previously not possible to do so. The methods are all measurement based, which means that no prior knowledge about the grid is required in order to compute the values.

Acknowledgments

There are many who have given me help and support during my studies, that deserve more appreciation than I am able to adequately convey.

First, naturally my family needs to be mentioned. The constant support throughout my life has been a true blessing. Mom, Dad, Christian, Stefan, you really have been the best anyone could ask for and for that I cannot be more grateful.

To all of my professors and colleagues, particularly Dr. De La Ree and Dr. Centeno, I truly am thankful for all of your guidance. You allowed me to search the world for what was really important to me, while still guiding me towards my goals. It is a rare gift that I have received and I will appreciate that forever.

Finally, to my close and dear friends, Jacques and Elliott, who have been with me this entire stage of my life. Your friendship throughout these years has perhaps been the most rewarding aspect of my studies. It is hard to imagine what it would have been like had I not met you two and no matter where we end up on our now separate paths, I will always remember and cherish the time we spent together.

Contents

List of Figures

List of Tables

Chapter 1

Introduction

The creation and maintaining of a robust and stable power grid has been of desire since the inception of the power system. However, as time passed and the power system has become much more complex, this task has similarly become increasingly complex. There are many factors which may affect the stability of a grid at any given time. The most common ways in which the system can become unstable are transient stability issues, voltage stability, frequency stability, and inter-area oscillations [1]. Because of all of these different ways in which the grid can become unstable, being able to determine if a given system is stable at any given time is of utmost importance.

There are several ways in which grid stability has been attempted to be quantified. Among the most common metrics for determining current grid stability are the H_∞ and H_2 metrics [2]. While these metrics vary in their approach, they make use of similar input quantities to make decisions. Particularly, the voltage and frequency deviations between buses are used to provide a metric for current system stability [3]. It has also been shown that grid inertia has an enormous impact on grid stability through its impact on the frequency response of the system [4]. Studies have also shown that when the sources of inertia are not evenly spread throughout the system, then the topology of the system plays a large part in the stability of the system [5].

With these parameters of inertia, topology, and voltage being necessary in order to quantify power system stability, the issue arises of how to obtain these quantities. Each quantity comes with its own separate challenge, yet all are needed in order to properly perform grid stability assessment. The major contributions of this work include:

- The development of a machine learning based procedure to estimate power system inertia constant values during steady-state conditions
- The ability to accurately estimate substation topology solely from synchrophasor data, without having to rely on breaker status information
- Improved estimation accuracy of voltage phasors in systems with reduced observability through the use of matrix completion optimization

1.1 Inertia Estimation

Inertia has a significant impact on the stability of the power system. The system inertia aids in maintaining the current conditions of the system, preventing events and small disturbances from rapidly changing the state of the system. The major source that provides inertia to the system is the rotating mass of machinery that is used in traditional energy sources such as coal or gas power plants. However, renewable energy sources such as wind or solar energy do not contribute to the system inertia.

This is becoming a large issue as ever increasing percentages of power generation are supplied by renewable energies. As these renewable energies get added to the system, the overall inertia will drop which makes the entire grid more susceptible to disturbances. Therefore, being able to estimate the value of the system inertia is becoming a necessity. Having the value of the inertia present in the system provides knowledge on the susceptibility of the current system and may enable the use of counter measures to prevent system instability.

Current methods used to determine inertia values, for example [6] and [7], rely on large system dynamic events, such as significant faults, to track the dynamic values in machines. While these techniques are accurate, their usage is very limited as large events do not occur frequently. Additionally, there are very large efforts being taken towards preventing large system events from occurring. Thus, using techniques which rely on these events is not ideal.

With the increased usage of phasor measurement units or synchrophasors in the system, there is much more information available about the current state of the system. With an increased amount of data available, the ability to determine the system inertia values during steady state operating conditions becomes a possibility. However, extracting the correct information that can be used for inertia estimation from synchrophasors can be a difficult process.

One possibility for the estimation of inertia is through the use of modal information. Modes of oscillation in electrical quantities arise in a system due to the slow mechanical oscillations of machinery against one another. These are the same machines that are responsible for adding inertia to the system; hence, using modal information as an input to the estimation procedure should be viable. There are techniques such as [8] which make use of modal information to determine the parameters, such as inertia, of the generators in a system. However, the aim of this work is to be able to incorporate all components in the system and obtain regional and complete system inertia values as well, not only generator parameter values.

The issue then becomes how to best use this modal information to estimate the desired parameters. When considering the complexity of the system, neural networks are a great tool for handling this problem. The field of machine learning has been growing rapidly and has made its way into a variety of fields, including power systems [9] or [10]. Most research, such as [10], focuses on using machine learning to predict future states of the system in techniques like load forecasting. The research proposed in [9], attempts to predict the load response of future events by using a neural network. The research into predicting the future

of the power system is extensive, yet the amount of machine learning used for real-time analysis is limited.

While there are many viable machine learning techniques, a neural network approach was selected, as opposed to other techniques such as state vector machines, for several reasons.With the power system being as complex as it is, the method needs to be able to handle these complexities. Neural networks are well equipped to handle very complex and particularly non-linear systems. This makes them an ideal tool for use in power systems. The major drawback being that neural networks do not allow for the user to view how decisions or calculations were made. Through this approach, estimating the inertia during steady-state conditions becomes possible, as seen in Chapter 2.

1.2 Topology Estimation

The state of a power grid is highly dependent on its topology. Analytics such as power flow or state estimation, as well as many others, require accurate knowledge about the connectivity of the system in order to obtain correct results. Normally the discussion of topology estimation revolves around the desire to determine which lines are in service and which are not. However, an equally important aspect of topology estimation is the connectivity of nodes within a substation.

Current topology estimation techniques make use of breaker status telemetry in order to determine substation connectivity [11–13]. Topology processors, such as the one suggested in [14,15], determine the topology for those parts of the system which have changed as compared to the previously processed topology. However, there are limitations on the availability and accuracy of this data. Many synchrophasor data systems do not have access to time synchronized breaker status telemetry, and those that do, have to deal with errors such as latching or other measurement errors. Thus, there is a huge financial burden on the deployment of synchrophasor analytics that require topology due to the required installation

of circuit breaker telemetry into the synchrophasor data stream.

Some systems make use of Supervisory Control and Data Acquisition (SCADA) system breaker telemetry in order to overcome this obstacle. However, there are several issues associated with this such as latency issues, lack of time synchronization, and the prevention of any redundancy with SCADA that would have been possible before. Additionally, the SCADA system is not time synchronized and the data obtained very infrequently. Through the increased availability of synchrophasor measurements, breaker statuses across nodes within a substation can be inferred or validated [16]. This can then be used in synchrophasor analytics, such as the Three Phase Linear State Estimator [17] or other state estimation applications, to improve their robustness.

There have been several previous approaches taken in an attempt to estimate substation topology. The work proposed by [18] uses synchrophasor data to validate breaker statuses. The breaker statuses are then used with a search procedure to determine the topology. Other techniques, such as [19], attempt to use a L1-norm state estimator in conjunction with a search algorithm to determine the topology. Other approaches attempt to detect errors in the assumed topology rather than to estimate the topology [20, 21].

The approach developed is a novel empirical method for determining the bus-branch topology of a synchrophasor based substation relying upon a phasor deviation threshold value. This threshold is determined based upon the concept of equipotential nodes within a substation. The deviation threshold can then be used to reconstruct the bus-branch topology of the substation. This procedure is detailed in Chapter 3.

1.3 Low Observability State Estimation

Observability in the power grid has been a constant issue since its inception. Knowledge of the present state of the grid allows for optimal grid operations. Traditional state estimation techniques require full network observability in order to produce accurate results. The most

common technique currently in use for state estimation is the Weighted Least Squares (WLS) algorithm [22]. While WLS does produce accurate results, it requires a high observability. Additionally, the WLS algorithm is limited to voltage, current, and power measurements.

However, obtaining the required observability for traditional state estimation, particularly in the distribution grid, is not feasible due to the immense scale of the network and limited availability of phasor measurement units (PMUs) [23]. Therefore, it has become imperative to be capable of estimating/completing the state of the grid for cases of *low-observability*, which roughly speaking means that the number of measurements is less than that of the quantities being estimated.

There has been much work done in an attempt to complete state estimation in situations where observability is an issue. [24] determines the optimal minimum measurement locations and then uses the difference between the measured and calculated voltages and complex powers to obtain the voltage profile of the whole network. [25] makes use of the voltage sensitivity at each bus to the load at all buses to determine the voltage given the measured load at each location. These approaches, however, still require the installation of significant numbers of PMUs when considering the scale of the system.

In order to improve the observability, methods for the optimal placement of limited number of meters have recently been investigated in, e.g., [26–28]; and methods that use pseudo-measurements and historical load profiles are proposed in [29–31]. [32] makes use of smart meter data to enhance observability of the system by solving the power flow over several consecutive time instances.

Machine-learning-based approaches are recently becoming popular for the task of state estimation in distribution networks. For example, [30, 33, 34] make use of neural networks to estimate the voltage in the network. These approaches have the benefit of not requiring a system model to obtain results, but retain the same consequences of all machine learning approaches, requiring significant amounts of data to obtain an accurate estimation.

Matrix completion is a well-established tool in the signal processing community for estimat-

ing missing values in low rank matrices [35]. It has been used within the power systems previously, in an attempt to do load forecasting in networks with incomplete data. For instance, [36] uses a correlation structure completion to fill in missing data for load forecasting; and [37] uses a kernel-based matrix completion approach that allows for the estimation of missing data even in locations where no measurements are available.

The methodology created in this work takes a matrix completion approach for estimating voltage phasors in networks with low observability. The original problem formulation for matrix completions is augmented with power-flow constraints which provide an additional link between parameter values. This *structured* approach has the following benefits compared to the existing techniques:

- It allows for voltage estimation from whichever measurements are available; as the number of measurement devices increase, regardless of quantity being measured, this data can be used as a supplement to estimate the voltage phasors in the entire system.
- The inclusion of power-flow constraints allow for smaller amounts of data required for accurate estimation compare to typical "black box" machine learning methods.
- The approach can be used to determine both voltage magnitude and phase angle in systems with few voltage phasor measurements.

The point of emphasis is that the versatility of the matrix completion approach allows for the use of *any* measurement that may be available in the field in order to perform state estimation. This is in contrast to many available techniques, such as [31, 32, 38], that make use of only voltage and real/reactive power measurements for the purpose of estimation. This allows for state estimation to be performed in systems that previously were unable to do so due to a lack of these measurements. The process for voltage estimation is shown in Chapter 4.

Chapter 2

Steady-State Inertia Estimation

Traditionally, the value of inertia is obtained through the equation

$$H = \frac{-\Delta P}{2\frac{df}{dt}} f_0 \tag{2.1}$$

where ΔP is the change in power that caused an event, $\frac{df}{dt}$ is the resultant rate of change of frequency, and f_0 is the system frequency at the time of the event. The value of H is the inertia referenced to the power rating of the bus such that it is possible to compare machines or buses of differing power levels, as seen in the equation

$$H = \frac{1}{2}\frac{J\omega^2}{S_{base}} \tag{2.2}$$

where J is the moment of inertia, ω is the rated angular velocity, and S_{base} is the rated power of the machine. Due to the physical nature of the quantity of inertia, it is much simpler to obtain its value during dynamic conditions due to the change in power and frequency being much easier to identify. However, this severely limits the opportunities for determining system inertia during normal power system operations since dynamic events are both infre-

quent and undesirable. Thus, estimating inertia during steady-state conditions has become necessary in order to be able to assess current system stability. When discussing inertia, there are several levels of inertia depending on the scope taken into consideration.

The smallest scale is the inertia of each individual bus in the system. This may provide some information, but is not as useful as the regional or total system inertia. The regional and system inertias are found through the combination of all the individual bus inertias through the equation

$$H_{sys} = \frac{\sum_{i=1}^{N} S_i H_i}{S_{sys}} \tag{2.3}$$

where S_{sys} is the summation of all rated powers within the scope. Through this it is possible to determine the inertia at various levels of scope. Thus, the method developed in this work attempts to determine the inertia at three different levels: the individual bus inertias, the regional inertias, and the system inertia [39].

2.1 Modal Information Extraction

The first step in the inertia estimation is to extract the modal information from the system. There are several methods for obtaining the modal information in a system. Many techniques, such as Prony analysis, require a disturbance in the system in order to obtain accurate results. Many of these techniques are thoroughly developed and are in widespread use. However, since the aim is to estimate values during steady state conditions these are not viable solutions for this specific problem.

There are a few methods for determining the modal information which do not require fault conditions for accurate calculations. These methods make use of ambient data from devices, such as synchrophasors, in an attempt to calculate modal information during small signal periods. However, these techniques are less well established than those that require fault

conditions. The technique proposed by [40] allows for the computation of modal information during steady state using information readily available from synchrophasors.

The technique proposed by [40] uses empirical mode decomposition in order to calculate the modes of oscillation. This method takes frequency data from the buses over a set time window and uses that to calculate the modal information. It is shown that if the window of data is large enough, the result of this method accurately represents the modal information in a system. The general algorithm for the technique is shown below.

1. Obtain the frequency value from each bus over a time window, removing the mean value from each data point, and compute the covariance matrix
2. Calculate the eigenvalues of this matrix and place into ascending order
3. Calculate the eigenvectors and normalize them
4. Determine the correct number of eigenvalues to ensure a significant amount of energy is captured by these vectors
5. Re-compute input data to guarantee accuracy of results

During steady-state operating conditions, the frequency in the system will have minor fluctuations due to small load changes. Additionally, due to the nature of the power system the frequency at all buses will not be equal. The frequency between buses will oscillate against one another. These oscillations and frequency deviations are recorded over a period of time in a window. Once the frequency of each bus over the time period is captured, each bus's data is placed into a matrix. An example of the created matrix can be seen below

$$X = \begin{bmatrix} f_{1,1} & \cdots & f_{1,j} & \cdots & f_{1,N} \\ \vdots & \ddots & \vdots & \ddots & \vdots \\ f_{i,1} & \cdots & f_{i,j} & \cdots & f_{i,N} \\ \vdots & \ddots & \vdots & \ddots & \vdots \\ f_{m,1} & \cdots & f_{m,j} & \cdots & f_{m,N} \end{bmatrix} \tag{2.4}$$

where $f_{i,j}$ is j^{th} measurement at bus i. From this matrix, once the mean value has been removed from each element, the covariance matrix C can be calculated through the equation:

$$C = \frac{1}{N} X^T X \tag{2.5}$$

Where N is the number of data points in each window and X is the matrix created from the collected frequency data at each bus, as seen in equation 2.4.

From the covariance matrix C, the eigenvalues and eigenvectors can be calculated. It is shown, that if the time window of the sampling is large enough these values will approach that of the real system. This window size required will vary for each application, but for power systems a window in the range of several seconds and larger is enough to obtain accurate results. The method described assumes that the system is linear, which is suitable for steady-state cases that have very small fluctuations.

2.2 Neural Networks

Using the modal information as an input to the system, a neural network was used to determine the inertia values. Neural networks make use of a combination of multiple simple decision techniques (notated as a neuron) to output an accurate solution for complex systems. As can be seen in Figure 2.1, each input parameter is input into every neuron, which then outputs a result that is combined with all of the other paths taken to create an optimal

solution. Each path is assigned a weight depending on the paths impact on the accuracy of the output.

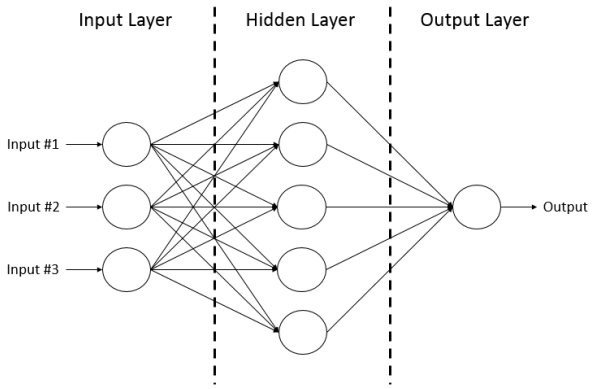

Figure 2.1: Example of a Neural Network

All of these decision paths are self-learned or trained using a portion of the data. When constructing the neural network, the complete data set is split into three categories: training data, validation data, and test data. As the name implies the training set is used to create or teach the neural network. The training set consists of giving the neural network both the input parameters and the outputs, allowing for it to construct the optimal path from the inputs to the outputs. The validation set is used to tune the parameters of the neural network, such as number of hidden layers and neurons. The network calculates the outputs given the set of input parameters and compares the outputs calculated to the actual outputs. The neural network is typically selected based on the best performance of the validation set. The test set is the final step of using the neural network on the desired data set and observing the accuracy.

Additionally, the parameters of the neural network were tuned to obtain the most accurate results. The tuning was done through the use of the validation set by the neural network as well as empirical iterations to determine the optimal network. The largest influence on the functionality of a neural network is the number of hidden layers and neurons used by the network.

The number of hidden layers used by the neural network can be seen as the number of simple decision metrics each path goes through. Each hidden layer will contain neurons which make decisions, then sends the decisions to the next layer. The number of neurons determines how many decision techniques are used within each hidden layer that are used in combination to produce an output. Increasing the number of neurons will increase the variety in decision approaches, but also increases the complexity of the network. Increasing the complexity of the network does not always improve the results of the network. The most accurate results were obtained through the use of a single hidden layer with 10 neurons in it.

Bagging was used to decrease the variance of the solution and to prevent overfitting. Since the result of neural networks is highly dependent on the starting conditions, results can vary highly. Thus, the variance of the output can be reduced through taking the average of several runs of the neural network. The final results that are shown in the following section are the average result of 10 runs of the neural network.

Finally, another method of early stopping was used while training the neural network to prevent overfitting of the data. Neural networks have a tendency to overfit the calculation procedure based on the specific input data. This is because the training of the neural network is an iterative process, meaning it will continuously run until the error on the specific input data is as low as possible. This will cause overfitting to the data and creates errors when applying the network to more general data. To overcome this tendency, the iterative process is stopped after a desired accuracy or number of iterations has been reached. The accuracy of the estimation on training and validation data is recorded overtime. The result with the most accurate validation results is typically selected. An example of this can be seen in Figure 2.3.

2.3 Simulations and Results

The methodology was tested on the IEEE 118-bus system using PSS/E. The system was split into three regions as seen in Figure 2.2. The regions were found based on the method described in [41], which makes use of graph theory to split the system.

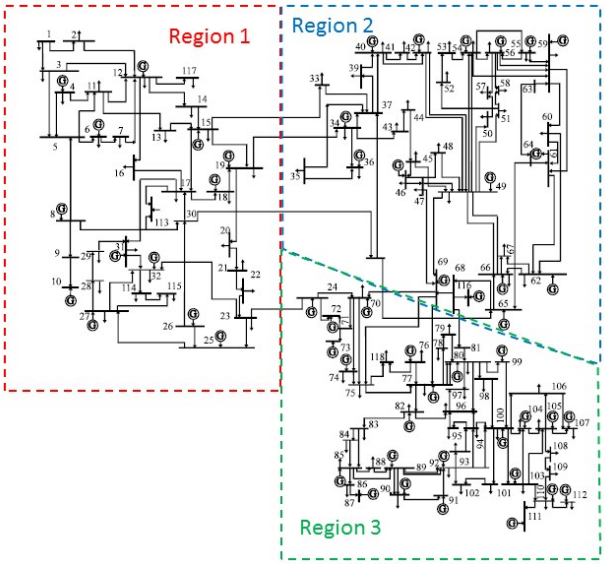

Figure 2.2: IEEE 118 Bus System with Regions Identified

To begin each simulation, the system inertia value was selected at random within a range of realistic values. From there, the regional inertia values were split randomly from the system inertia. The inertia values of the generators and rotating loads within the system were then randomized, maintaining a range of 2s to 8s. This was to ensure that the system would maintain stability during simulation and that the inertia values are realistic. The system would then be simulated for a long duration under realistic steady-state conditions in PSSE.

The minor fluctuations in the frequency present in realistic systems during steady-state were created through the use of minor load fluctuations during the simulation. At various random bus locations throughout the system, the existing load was altered to a new value by increasing or decreasing the value by a small percentage of the base load following a normal

distribution. This was done periodically such that the behavior of the system resembled a realistic system during steady-state.

The frequency from each bus over a time window of two seconds was taken in order to calculate the modal information with the method described in section 2.1. To resemble actual PMU data, the measurements were taken 30 times per second. This time window was found to be large enough that the eigenvalues and vectors calculated through this method were an accurate approximation to the modal information of the system. For each bus in the system, the first four modes of oscillation were recorded. It was found that typically most of the energy present in the signal was contained in the first four modes of oscillation, thus this number of modes was selected. The inclusion of additional modes did not improve the accuracy of the output.

Once the modal information was found, the inertia values of that specific simulation were stored in pair with the modal information of the system obtained. This process was repeated for hundreds of cases to achieve a sizeable data base to allow for accurate results from the neural network analysis. The data was split randomly into the three groups of train data, validation data, and test data. As the names imply, the neural network was creating and trained using the train data, attempting to have the results as close to the validation data while being cautious of overfitting. The results that are output can then be compared to the test data to see the accuracy of the network.

The neural network was run with each mode of oscillation individually, and then with all modes included. The most accurate results were found when using all possible modal information as an input. The results of this procedure can be seen below. Figure 2.3 shows the accuracy of the neural network versus training time.

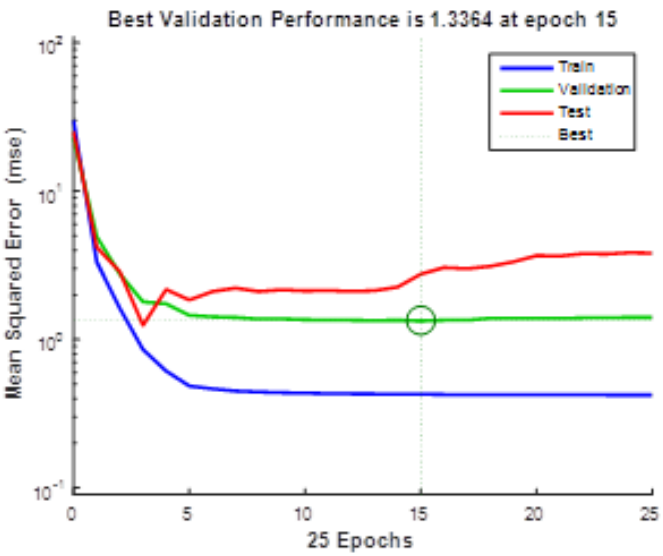

Figure 2.3: Accuracy of Neural Networks as Training Time Increases

Each epoch is an iteration through the training procedure on the data. It can be seen that the accuracy of the training and validation sets reaches optimal accuracy at around 5 epochs, however the accuracy of the neural network on the test data begins to decrease after the 5th epoch as well. This is due to the problem of overtraining of neural networks. Each iteration tunes the neural network to work more accurately for the data set given, which reduces the generality of the network causing it to work less well on other data sets. As a result, the training of the neural network should be stopped between 5 and 15 epochs for optimal results, in this case 15 epochs was used due to having the highest accuracy in the validation set.

Figure 2.4 shows a histogram of the errors between calculated values and the actual values. Most of the errors are near to zero, while a few are slightly larger. This is true for all of the data sets: training, validation, and test data. However, as the inertia values do not vary drastically in realistic systems, these small differences can signify significant errors.

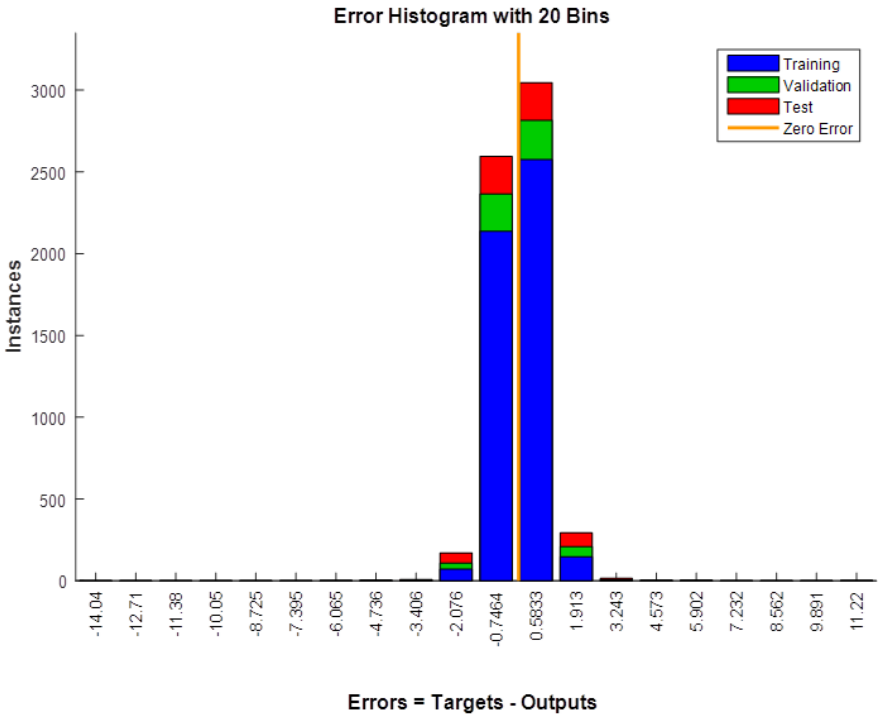

Figure 2.4: Neural Network Errors

Figure 2.5 shows the distribution of the errors between each estimate and the actual value.

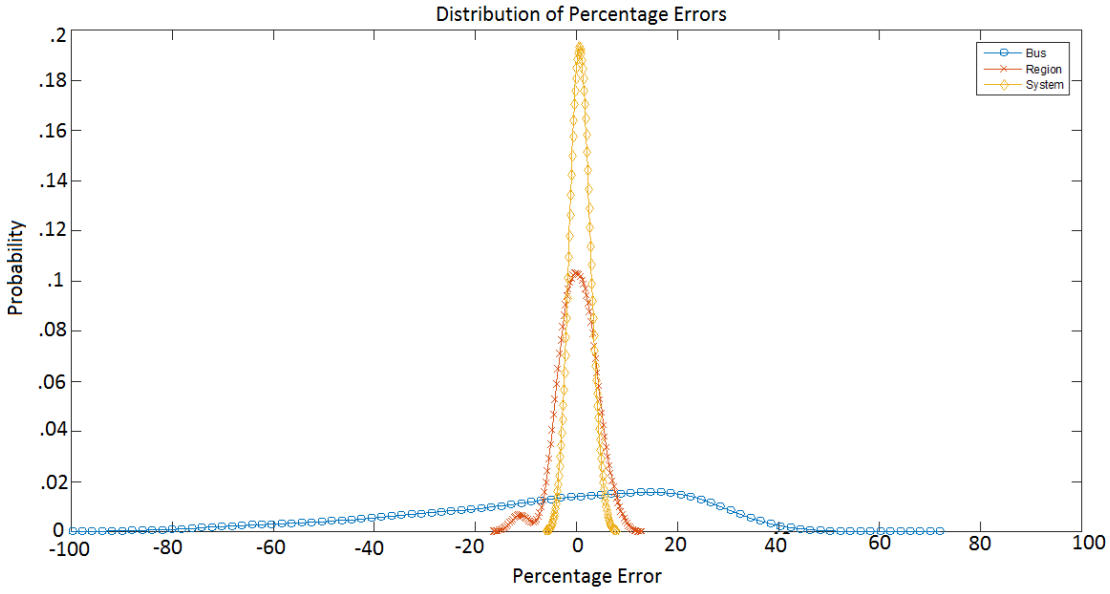

Figure 2.5: Distributions of Estimation Errors

Table 2.1: Mean Absolute Percentage Error of Inertia Estimations

	Individual Bus Inertias	**Regional Inertias**	**System I**
MAPE	21.5%	2.8%	1.4%
Standard Deviation of Percentage Errors	26.89%	3.62%	1.65%

It can be seen from this, that the neural network accurately identifies that regional and system inertias, but assigns the average value of inertia to the individual buses such that these regional and system inertias are obtained. Table 2.1 shows the mean absolute percentage error (MAPE) and standard deviation for each case. MAPE is calculated through the following formula:

$$MAPE = \frac{100}{n} \sum_{i=1}^{n} \frac{ActualValue_i - EstimatedValue_i}{ActualValue_i} \tag{2.6}$$

Where n is the number of data points calculated.

In these cases, bus inertia is defined by the combined inertia of any rotating masses attached to the bus, such as generators or machine loads. If a bus did not have any rotating masses connected to it, then it was not considered in this work.

It can be seen from these results that the estimation of the individual bus inertias is not accurate. The mean absolute percentage error of the individual bus inertia estimation results is 21.5%. This is a very large error and as a result the estimates for individual bus inertia are not usable. It is also of note that the standard deviation of the errors for the individual bus estimations was very large. This indicates that this procedure was not able to find a strong enough relation between the calculated modal information and the inertia values at the buses. There are a few reasons for as to why the neural network is not able to estimate individual bus inertias accurately.

The correlation between modal information and inertia may not be strong enough for accu-

rate estimation. That is to say, the inertia at the buses may not have had a large enough impact on the modal information in the system for the neural network to detect the changes in the modal information when different inertia values were used. It is possible that including other variables in addition to the modal information would be beneficial. Another alternative could be to attempt to determine under what circumstances the bus inertia estimations would be accurate. This could possibly be done through the use of participation factors or sensitivity analysis.

However, when looking at the entire system inertia values or the regional inertia values the results are much more accurate. The mean absolute percentage errors for the regional and system inertia estimates are 2.8% and 1.4% respectively. Additionally, the standard deviation of the errors was low for both of these cases. While calculation of individual bus inertias is desirable, the results from the regional and system inertias are important and can be used for analysis on the system which, ultimately, is the objective.

The results show that this method is usable for the estimation of regional and system values. However, it is not able to accurately estimate the values of the inertia at individual buses within the system.

Chapter 3

Empirical Topology Estimation

When discussing topology, most people will first consider how all the substations are connected to each other through transmission lines. However, another factor which also has a significant impact is how each substation is connected internally at any given moment. Most topology estimation techniques make use of circuit breaker statuses in order to obtain the topology. For example, in Figure 3.1, it can be seen that since two breakers are open, while the other two are closed, two buses within the substation have formed.

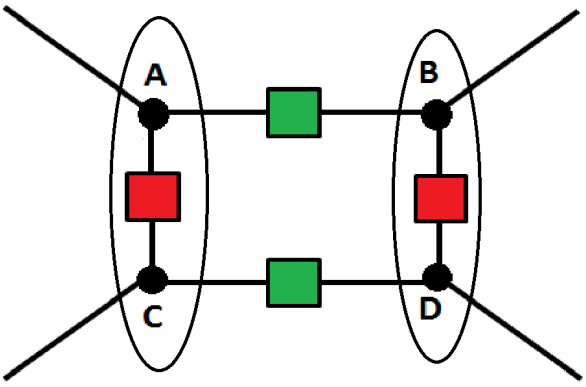

Figure 3.1: Example of Node Groupings

However, the issue is that this information is not normally available in synchrophasor data

streams in the vast majority of systems. This means that any synchrophasor analytic, such as state estimation, that relies upon the knowledge of topology in order to accurately function has to obtain this information from other sources. This severely limits the functionality of synchrophasor analytics in these systems.

Unfortunately, the reason that the circuit breaker status data is so often not available in synchrophasor data streams is because of the huge investment burden of the cost to install all of the equipment required. Therefore, to alleviate this burden a methodology was devised such that system topology can be estimated solely with the use of synchrophasors with relatively high accuracy. This allows for the use synchrophasor-only analytics, which do not need to rely on any other types of data sources [42].

3.1 Threshold Calculation

The first step in the procedure is to determine a voltage phasor deviation threshold, such that it is safe to say that any nodes which have a difference in their voltage phasors larger than this threshold are not connected. This deviation threshold is obtained empirically making use of the concept of voltage coherency [43].

Voltage coherency is the idea that nodes which are connected should have ideally the same, but at the very least extremely close, voltage phasors. This can be seen best while observing phase angles, thus going forward all discussion will be focused on phase angles rather than magnitudes. With this in mind, it should be possible to observe in a system the "normal" differences in phase angle that disconnected nodes have. If this value can be obtained, then it should be possible to say whether two nodes are connected or not with relative certainty.

The way in which the threshold is obtained is through the running of simulations in order to obtain the difference of angles across disconnected nodes for all possible system configurations and then run a statistical analysis on the acquired data to best select a value for the threshold. This does, however, mean that the phasor deviation threshold value obtained is specific to

the system upon which the analysis is done.

The issue of how to determine the voltage phase angle deviation threshold from this information must next be solved. While ideally any two nodes that are connected by a breaker will have the same voltage phasor, this is not the case in a real system. There are several factors that may cause the voltage phasors to differ. The most likely cause and factor of highest impact is measurement errors. Any measurement in a real system will have an associated error with it due to various issues, such as noise, poor calibration, quantization, etc., that will make comparisons of values more difficult.

Another cause of disconnected nodes maintaining similar voltage phasors is the connectivity of the system. It is possible for very short paths between two nodes to exist outside of the substation which will cause the voltage phasor values to stay relatively close even if they are disconnected.

Thus, because of these issues, when determining the phasor deviation threshold, it needs to both be small enough to accurately determine the connectivity state of nodes in the vast majority of cases, while being large enough to avoid misclassifying connections due to these issues. As such, it was chosen to use a value such that 95% of all phase deviations recorded were above the threshold. It will be shown later, that even with this criteria, the voltage phase deviation threshold is relatively large, which confirms the assumptions made that nodes that are disconnected will have differing voltage phasor values.

The system that is used for this work is the IEEE standard 118 bus system, as seen in Figure 3.2. However, since this topology estimation procedure attempts to determine the connections within a substation, this system needs to be modified to be of use. As such, there are two approaches used for the creation of a system that contains substations. The first method transforms each bus within the IEEE 118 bus system into a substation with one of four different standard layouts, while the other method is a more general black box approach, which has been named the synthetic mesh method.

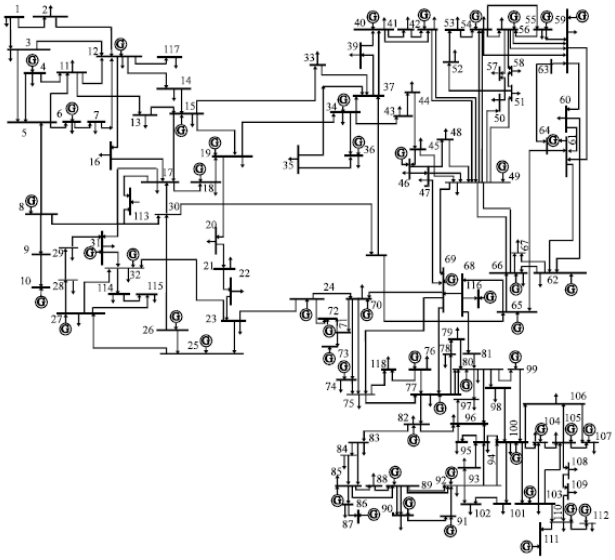

Figure 3.2: IEEE 118 Bus System

3.1.1 Standard Substation Topologies Approach

Within power systems, there are several standard substation topologies or layouts in use. These topologies are:

- Double-Breaker, Double-Bus
- Breaker and a Half
- Ring Bus
- Single Breaker, Single Bus

and can be seen in Figure 3.3.

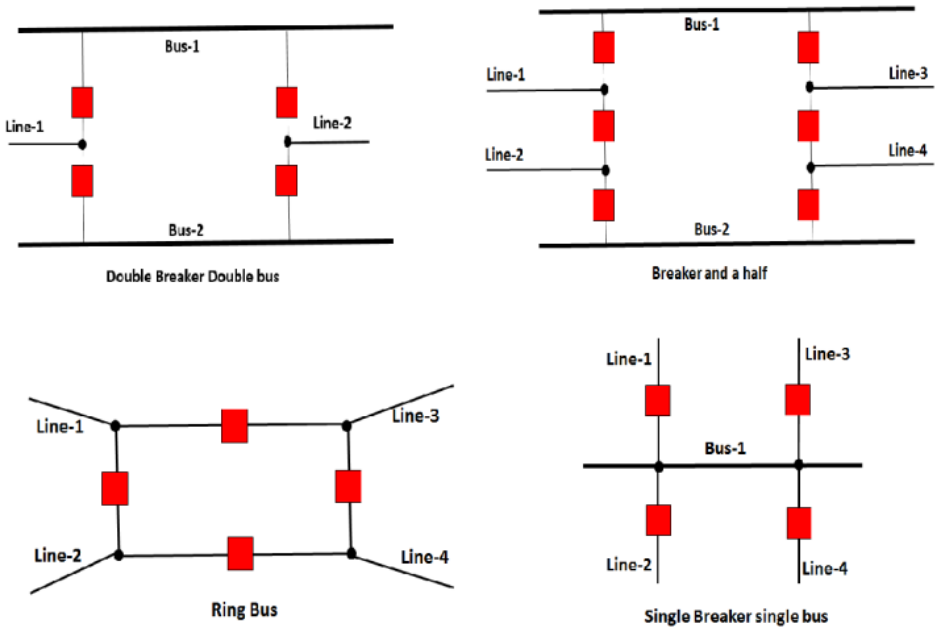

Figure 3.3: Standard Substation Configurations

With this information, every bus within the 118 bus system was modified into one of these substation topologies, such that each component(transmission line, machine, load, etc.) connected to the substation is connected to an individual node within the substation. With this system created, all possible connection cases the system substation topology connections can be tested.

The simulations were run and the phasor variation threshold was found as described previously. Figure 3.4 and 3.5 show the histogram and cumulative distribution function of the recorded angle deviations, respectively.

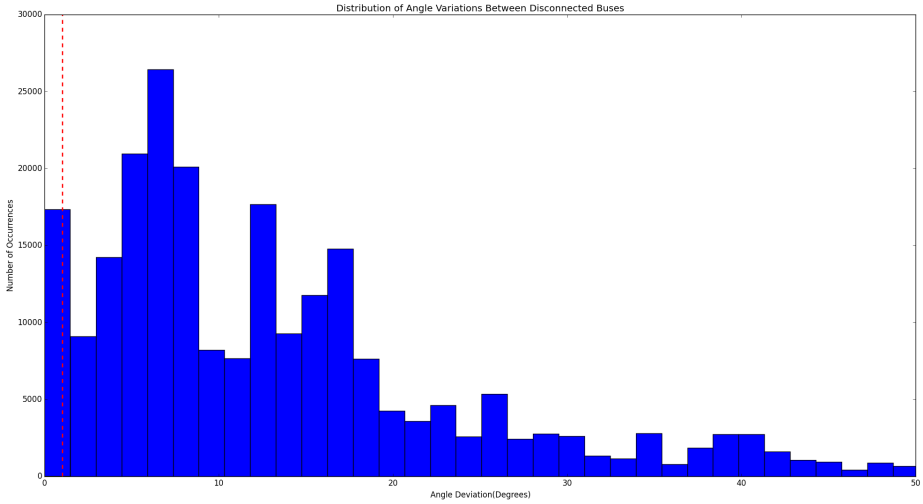

Figure 3.4: Histogram of Phase Angle Deviations in the Standard Substation System

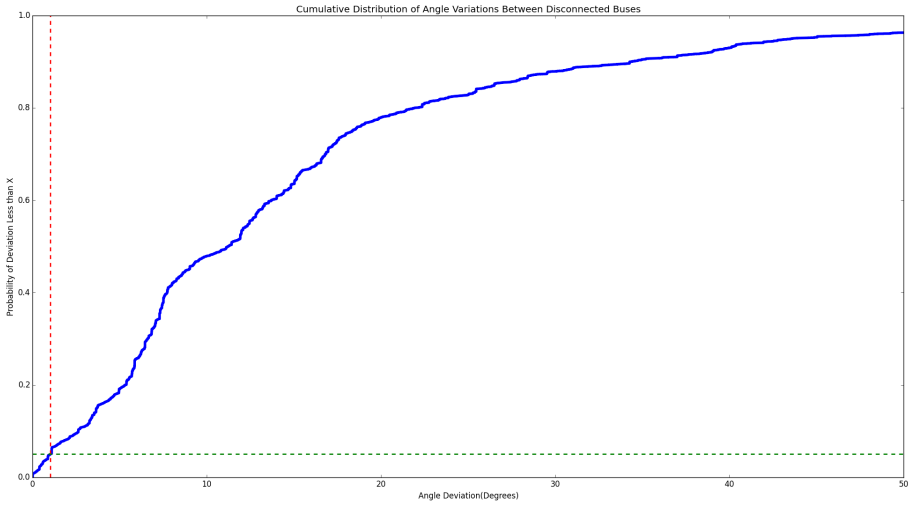

Figure 3.5: CDF of Phase Angle Deviations in the Standard Substation System

From these plots, it can be seen that when selecting a threshold value for which 95% of cases are larger, the threshold is **1.01**°. This is a desirable value for a few reasons. First, it confirms the assumption that when two nodes are disconnected, the voltage phasors will

be different from one another. Secondly, the value is large enough to be able to account for noise with relatively high accuracy. From the synchrophasor measurement standard, it is required that all synchrophasors have a measurement total vector error under 1% [44]. In the worst case scenario, which should be stated is highly unlikely, that the entirety of this error is applied to the phase angle, the measurement error for phase angles can only be as large as .517° [44]. Therefore, for there to be a misclassification due to measurement errors, both measurements would need to have the highest worst case scenario error on their measurements in opposite directions, which is extremely unlikely.

Additionally, since the individual substations are modeled both the threshold for each type of standard substation layout, as well as the potential threshold for each individual substation can be found. Figure 3.6 and 3.7 show the histogram and cumulative distribution function for each type of standard substation configuration respectively.

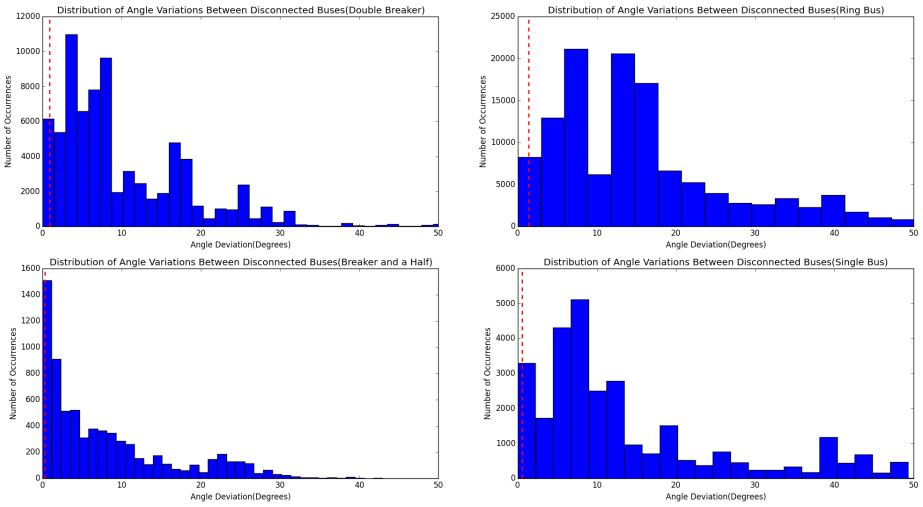

Figure 3.6: Histogram of Phase Deviations for Each Substation Type

Table 3.1: Phasor Deviation Threshold for Each Standard Substation Type

Substation Type	**Deviation Threshold**
Double-Breaker, Double-Bus	0.87°
Breaker and a Half	0.27°
Ring Bus	1.40°
Single-Breaker, Single-Bus	0.58°

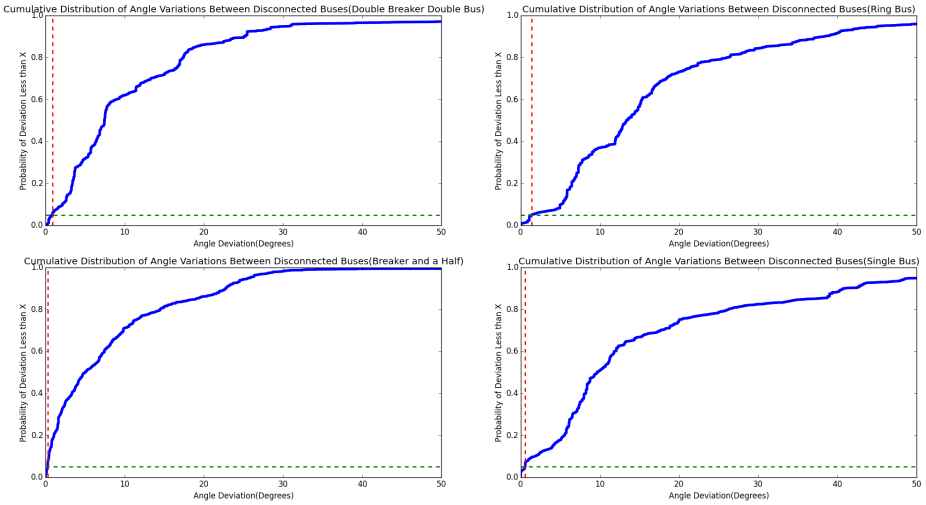

Figure 3.7: CDF of Phase Deviations for Each Substation Type

The threshold of each type of standard substation configuration can then be found and is shown in Table 3.1. From this it can be seen that while the type of substation layout does have an impact on the threshold value, it is not significant. There may be issues with the value of the breaker and a half threshold, but it is still not unreasonable.

If each substation is considered individually, the resultant threshold for each individual substation can then be seen in Figure 3.8. Through this, the variations and importance

of substation location become more apparent. However, it can be seen that the phasor deviation threshold for the vast majority of substations can be set significantly large.

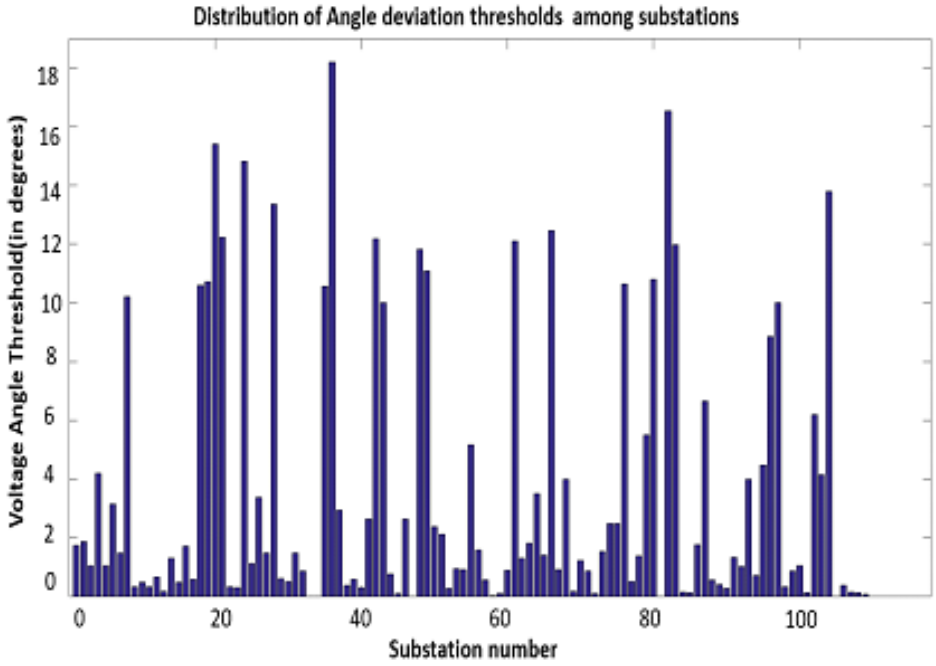

Figure 3.8: Threshold Result for Each Individual Substation

Finally, to verify that the results are plausible on other systems, similar studies were run for the IEEE 14 bus system as seen in Figure 3.9.

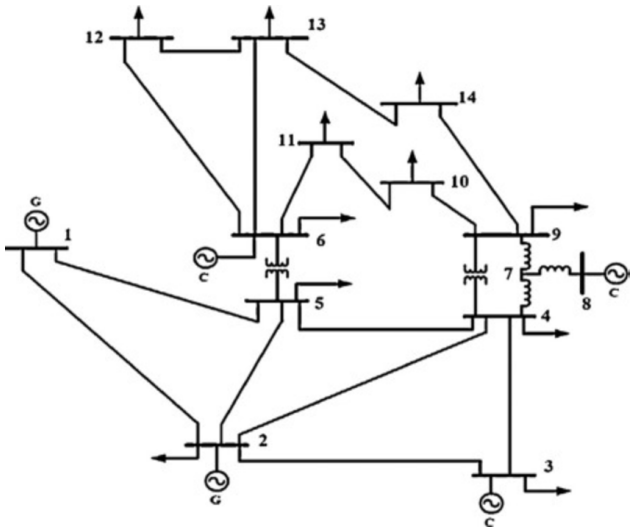

Figure 3.9: IEEE Standard 14 Bus System

Figures 3.10 and 3.11 show the histogram and cumulative distribution function respectively.

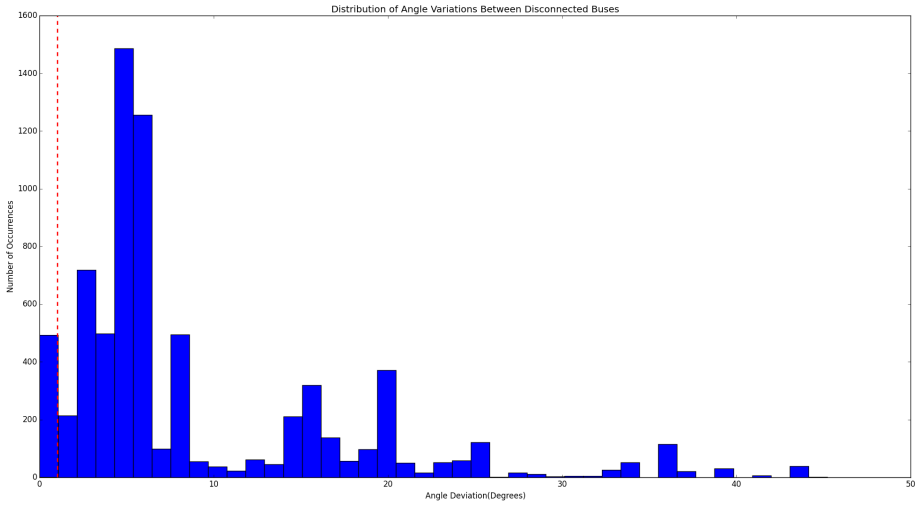

Figure 3.10: Histogram of Phase Deviations for the 14 Bus System

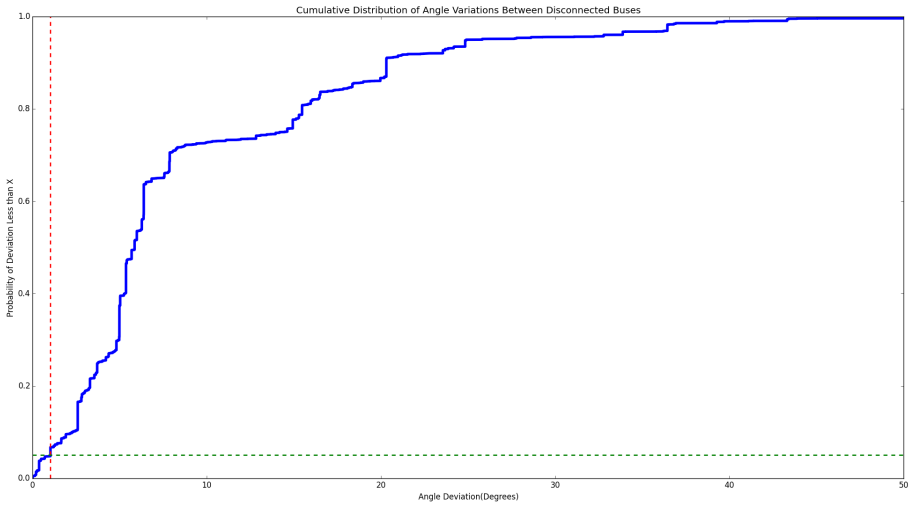

Figure 3.11: CDF of Phase Deviations for the 14 Bus System

From these plots, it can be seen that the voltage phasor deviation threshold is 1.03°, which is also a desirable value. This also shows that the size of the system is not a determining factor in the value of the phasor deviation threshold.

3.1.2 Synthetic-Mesh Approach

The synthetic mesh approach does not assume knowledge of any connections between the nodes within the substation. It works under the assumption that any node within the substation can be connected to any other node, as seen in Figure 3.12. Through this, every possible node connection case is tested and the phase angle between disconnected nodes are recorded.

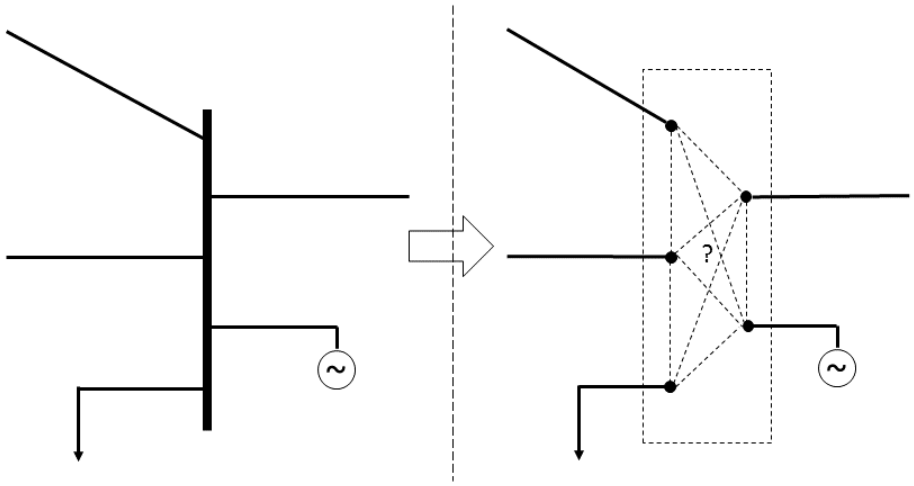

Figure 3.12: Synthetic Mesh Substation Example

Once again, all simulations were run and the results can be seen in Figure 3.13, which shows a histogram of the phase angle deviations.

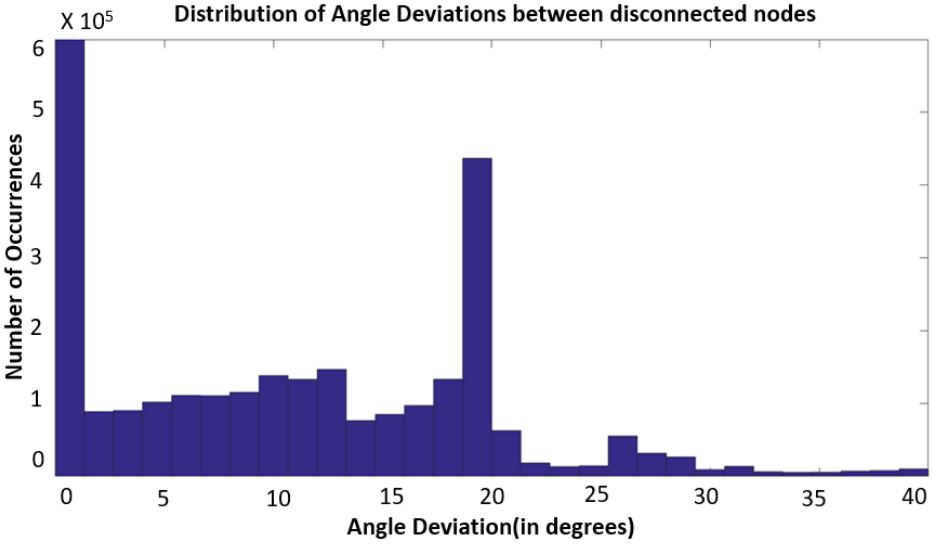

Figure 3.13: Histogram of Angle Deviations for the Synthetic Mesh Approach

In the same process as before, the deviation threshold was selected such that 95% of all deviation cases were above the threshold. For the synthetic-mesh approach, this results in a deviation threshold of 0.75°. While still large, this value is lower than the standard

substation topologies method. This is due to the increased connectivity of the system being tested. However, the value is still viable and able to produce accurate results.

3.2 Topology Estimation

Once the voltage phasor deviation threshold has been found, the topology of the substation can be estimated. The procedure has been split into several levels that build upon the output of the previous levels by making additional assumptions. This was done in this manner such that the user can select which assumptions they are comfortable with and have confidence in the result.

While there will be much discussion about inferring breaker status correctly, it should be noted that this is not the end goal. There are cases where a specific breaker's status is irrelevant in correctly determining the topology of the substation. The objective of this procedure is to construct the bus-branch model of the system from the nodal-breaker model, thus the final output of the estimation is the topology of the substation, not necessarily the breaker statuses.

3.2.1 Level 0: Initialization

The first level makes no assumptions about the connection between nodes. It solely takes into account the voltage phasor measurement where available and determines whether each node is energize or not. Each individual energized node forms its own bus, unenergized nodes are disconnected, and unmeasured nodes are considered unknown or unobserved.

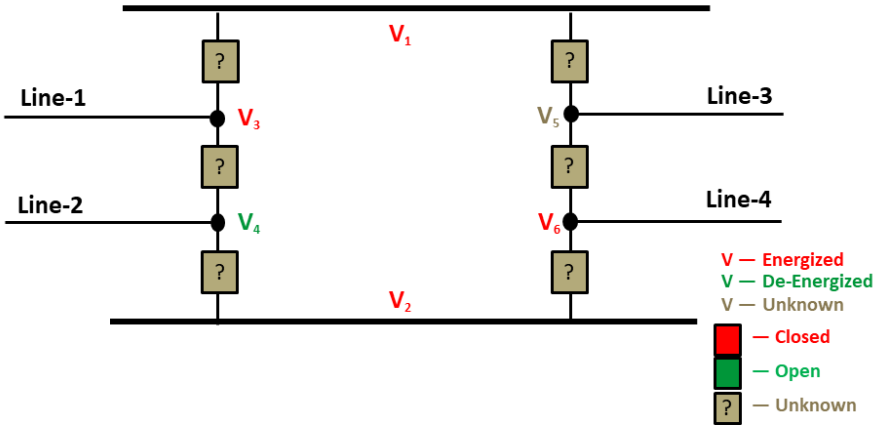

Figure 3.14: Example of Level 0 Topology Estimation

As seen in Figure 3.14, for this level nodes V_1,V_2,V_3,V_6 are energized forming four separate buses, while node V_4 is not energized, thus not connected inside the substation. Additionally, since there is no measurement at node V_5, this node is marked as unobserved.

3.2.2 Level 1: Read Breaker Status Telemetry(If Available)

While the intention is to estimate topology without the use of breaker statuses, it would be foolish to not use the information if it is available. This level makes use of breaker status telemetry, when available, in order to determine connectivity between nodes.

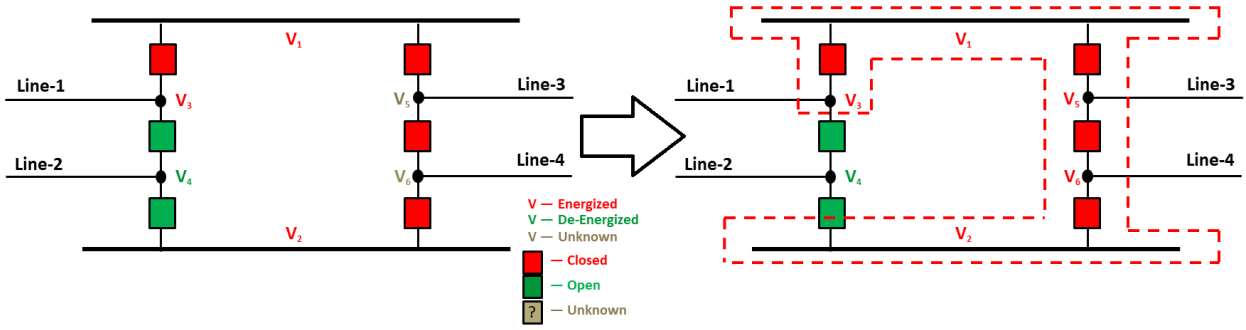

Figure 3.15: Example of Level 1 Topology Estimation

As seen in Figure 3.15, for this level nodes V_1 and V_3 are connected and form a bus, and the node V_2 is known to be energized. Additionally, while V_5 and V_6 are unknown, since the breaker statuses are measured as closed these two nodes are determined to be connected to the bus containing nodes V_1,V_2,V_3,V_5,V_6. Node V_4 is both unenergized as well as the breakers known as open, meaning that the node is not connected within the substation.

This is the ideal case when all breaker statuses are known. For example, had the breaker between nodes V_5 and V_6 not been known, it would have been impossible to say for certain if all five nodes are contained in a single bus or if there are two separate buses containing two and three nodes respectively. Alternatively, if any of the breakers in the right section of the substation were unknown, it would create uncertainty and cause the topology estimation to be incomplete when using incomplete breaker status telemetry.

3.2.3 Level 2: Infer/Validate Breaker Status

Level 2 is where the previously obtained phasor deviation threshold is first used. In this level, adjacent nodes that both have voltage estimates are compared. If the difference is larger than the threshold, the nodes are considered disconnected and the breaker open and vice versa.

If there is no information on the breaker status previously, then the status is assigned to open or closed, depending on the voltage difference. If there is a previously known status and the voltage difference determines the same status, then the state is validated in this level. If the newly determined status differs from the previously measured status, a flag is thrown to alert the user. In the current implementation, the voltage difference method takes precedence over the breaker status telemetry. However, this is easily modifiable.

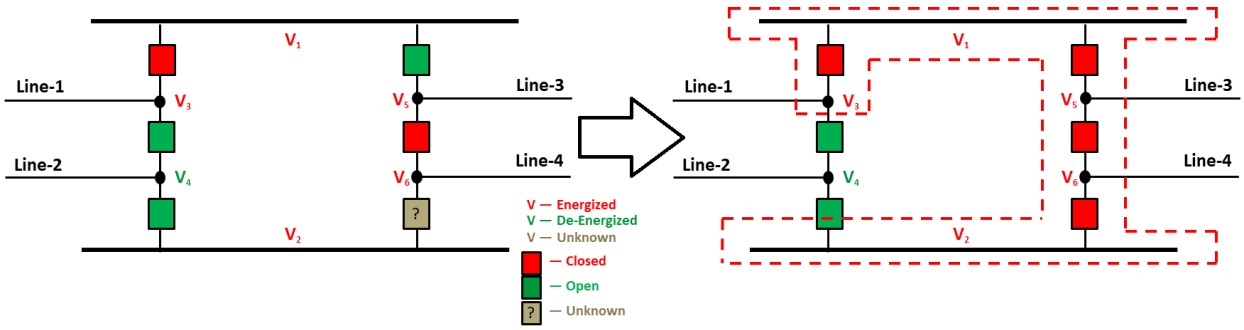

Figure 3.16: Example of Level 2 Topology Estimation

It can be seen in Figure 3.16, that even though the breaker is unknown between nodes V_2 and V_6, it can be inferred that it is closed by the proximity of the voltage phasor between the two nodes. Additionally, it is found that the breaker between nodes V_1 and V_5 has the incorrect status, throwing a flag to let the operator know that they need to investigate further. Without the inclusion of voltage phasor comparisons in this level, the topology would have been wrongly determined when only using breaker status telemetry.

3.2.4 Level 3: Voltage Coherency

This level does not make use of breaker status telemetry at all. It solely looks upon the voltage phasors values of all known nodes and groups them based upon voltage coherency making use of Jenks Natural Breaks Optimization.

Jenks Natural Breaks Optimization is a clustering technique that looks for natural breaks in one dimensional data. It is a single dimensional K-means clustering approach. This method attempts to minimize the average deviation from each clusters mean and maximize the separation between clusters. This process is iterative to determine which break locations result in the optimal clusters. The methodology works as follows:

1. Split data into arbitrary initial groups

2. Calculate the sum of squared deviations for each cluster

3. Calculate the sum of squared deviations for the complete data set
4. Subtract the results of Step 2 from the results of Step 3.
5. One data point is then moved from the cluster with the largest value obtained from Step 4 to the cluster with the smallest value.
6. Return to Step 2 until the results from step 2 are below a set threshold
7. Repeat process while increasing number of clusters until the goodness of fit is above a set threshold.

This process will cluster the data into groups based on the proximity of voltages. Naturally, as the number of clusters increases the goodness of fit will increase but the increase is not linear. It is necessary to stop the iterations after a threshold has been reached or the algorithm will continuously create new clusters when there should not be any. However, if the the goodness of fit threshold is properly tuned, the results of the jenks natural breaks optimization will return the proper node clusters with relative accuracy.

3.2.5 Level 4: Complete Combination

This is the final level, building upon the output of level 3, but includes breaker status telemetry when available, as well as uses knowledge of the layout of the substation in an attempt to connect unobserved nodes. This is the most inclusive of levels, but also makes the most assumptions about what allows for the determination of connectivity.

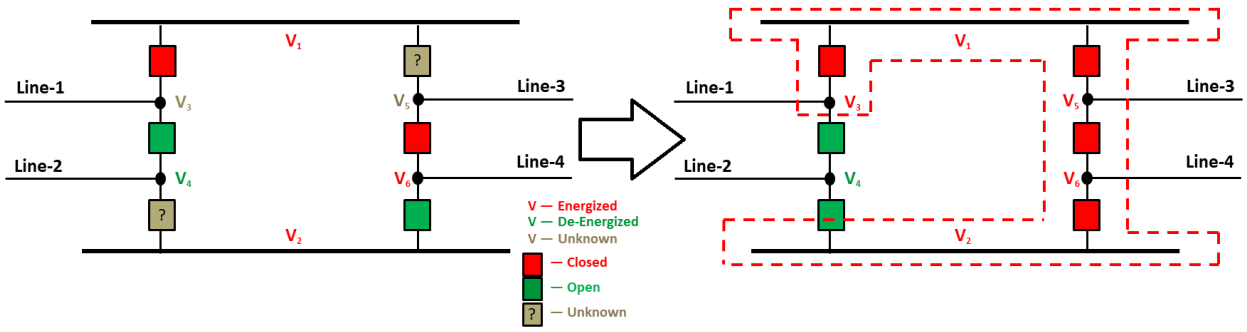

Figure 3.17: Example of Level 4 Topology Estimation

For example, in Figure 3.17, nodes V_3 and V_5 are unknown. Additionally, the breaker status between nodes V_2 and V_4 as well as between nodes V_1 and V_5 is unknown. Through the closed breaker status of the breaker between nodes V_1 and V_3, it can be determined that nodes V_1 and V_3 are connected. Similarly with nodes V_5 and V_6. Combined with the voltage coherency grouping obtained from the results of level 3, it can then be seen that nodes V_1,V_2,V_3,V_5, and V_6 are all connected, while node V_4 is isolated from the substation. Finally, with these groupings determined it is noted that the breaker between nodes V_2 and V_6 has the incorrect status and a flag needs to be set for this breaker. Finally, the breaker between nodes V_2 and V_4 can be set to be open.

3.3 Simulation and Initial Results

This algorithm was initially implemented and tested with python in conjunction with PSS/E, in order to determine the validity of the process before incorporating it with other softwares or algorithms that rely upon topology. Roughly 40,000 simulations were run, each with a random system topology and loading. The accuracy of the estimation process can then be determined by comparing the output of each level to the actual topology. For each simulation, the estimation was determined to be successful if, and only if, the topology was estimated perfectly correctly. Any small, even minute, deviations from the actual topology were still

considered as an incorrect estimation. The accuracies for estimation at each substation for level 3 and level 4 can be seen in Figure 3.18.

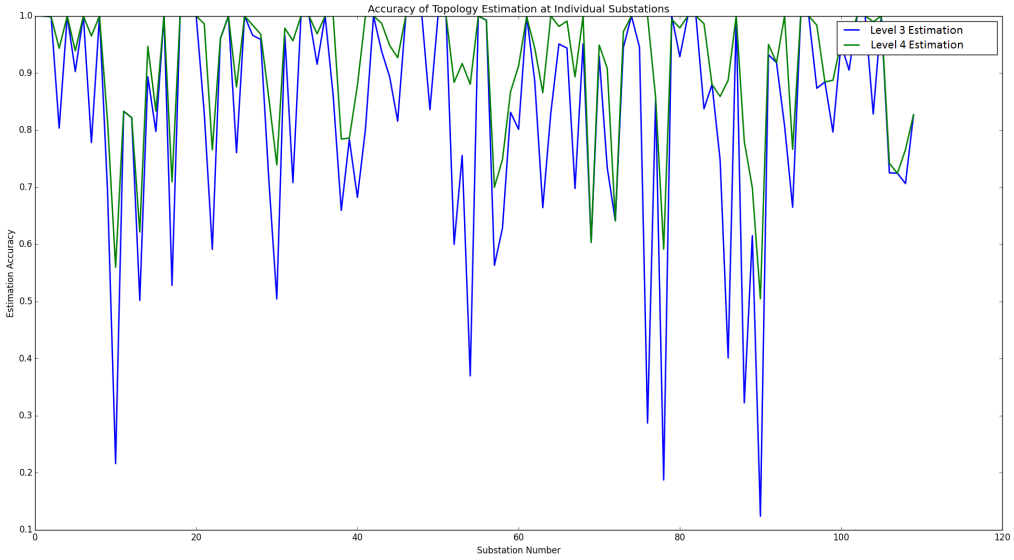

Figure 3.18: Accuracy of Topology Estimation Procedure at Each Substation

It can be seen that the accuracies are relatively high for all substation, particularly at level 4. The large discrepancies between level 4 and level 3 accuracies in certain substation are due largely to the size of the substation. Since level 3 estimation solely makes use of voltage coherency and does not take into account the layout of the substation, as the substations grow in size the number of possible connections increases, which drastically increases the possibility of an incorrect estimation under the criteria used to determine success.

Additionally, the impact of noise was tested to once again verify the assumption made in regards to the viable of using a voltage deviation threshold. As stated previously, the maximum noise allowed by the IEEE standard is 1% total vector error on the phasor, which when applied entirely to the angle is 0.517 degrees [44]. While this is an almost unrealistic worst case error, it is useful in testing the impact of measurement error. Assuming the noise follows a normal distribution, error was added to the results of all of the simulations for both

Table 3.2: Estimation Accuracy of Two Different Algorithm Levels with Varying Noise

	Level 3 Accuracy	**Level 4 Accuracy**
No Measurement Error	0.866	0.928
1% Measurement Error	0.851	0.918
3% Measurement Error	0.682	0.573

1% and 3% error. The accuracies were recorded once again for both level 3 estimation and level 4 estimation. The resultant accuracies can be found in Table 3.2.

From this table, it can be seen that even at a worst case error of 1% both levels have a high accuracy in determining the actual topology. As the error increases beyond the allowable measurement error, level 3 becomes more accurate. This is due to the strict criteria used in determining success or not. Level 4 will compare phasors of connecting nodes, so a single difference caused by error between any of the nodes will cause the estimation to be unsuccessful. Level 3 is more forgiving in that voltages are compared collectively without regard to layout allowing for the mitigation of incorrect estimations due to measurement errors.

It should be emphasized that these accuracies are not for the portion of time that the estimation procedure was correct. The accuracies show the fraction of possible system configurations that the estimation was able to correctly determine. It does not take into consideration the amount of time or frequency of occurrence for each case. So while there may be cases that the procedure is not able to determine correctly, these cases may be rare and never realistically occur during normal system operation.

3.4 OpenECA Platform and Implementation

Finally, this algorithm was implemented through the OpenECA Platform as part of the Linear State Estimator [17]. The Open and Extensible Control and Analytics(openECA) Platform is a an open source platform which can be used to simulate the transmission of data in real-time to an application [45]. This allows for the testing of applications under realistic system conditions with much greater ease and greatly increases the speed of development and implementation of such analytics into the actual system.

The entire algorithm is publicly available on the openECA github page.

Chapter 4

Low Observability State Estimation

Voltage phasors are the most commonly and widely used value, impacting most aspects of the power system. As such, there has been a lot of work done in order to obtain the voltage values. The difficulty in estimating the voltage is the required observability of measurements needed to accurately view the whole system. The approach presented uses matrix completion in order to estimate system voltage phasors under situations of low observability [46].

4.1 Matrix Completion

The goal of matrix completion is to determine the unknown elements of a matrix, given a low rank matrix with a set of known elements Ω. The difficulty lies in the required number of observations and the assumption of low rank. Since missing elements are being estimated through the use of known elements, there both has to be enough known elements to make such an estimation possible and a correlation between the elements in order to obtain an accurate estimation.

We next define the matrix completion problem formally. Consider the space of real-valued $n_1 \times n_2$ matrices $\mathbb{R}^{n_1 \times n_2}$. Let $\mathcal{I} := \{1, \ldots, n_1\} \times \{1, \ldots, n_2\}$ denote the index set, so that

$(i, j) \in \mathcal{I}$ represents an element's index. For any matrix $W \in \mathbb{R}^{n_1 \times n_2}$ and a subset $\Omega \subseteq \mathcal{I}$, let W_Ω denote

$$W_\Omega = \begin{cases} W_{i,j}, (i,j) \in \Omega \\ 0, \text{otherwise.} \end{cases} \tag{4.1}$$

Let M be the original matrix to complete, Ω be the set of elements with observed values, and M_Ω be the observation matrix, such that elements where data is available are set to the observed value and the remaining are set to zero. From [35], the problem of matrix completing can then be formulated as a rank minimization problem:

$$\begin{aligned} \min_{X \in \mathbb{R}^{n_1 \times n_2}} \quad & \text{rank(X)} \\ \text{s.t.} \quad & X_\Omega = M_\Omega, \end{aligned} \tag{4.2}$$

However, it can be seen that the formulation of (4.2) is a non-convex, NP-hard optimization problem to solve, which makes it unusable for implementation. An alternative approach to circumvent this problem is to minimize the *nuclear norm* of the matrix:

$$\begin{aligned} \min_{X \in \mathbb{R}^{n_1 \times n_2}} \quad & \|X\|_* \\ \text{s.t.} \quad & X_\Omega = M_\Omega, \end{aligned} \tag{4.3}$$

where

$$\|X\|_* = \sum_{i=1}^{n} \sigma_i(X) \tag{4.4}$$

and $\sigma_i(X)$ is the i^{th} singular value and $n := \min\{n_1, n_2\}$.

There has been work done recently to improve on the accuracy of this algorithm. Reference [47] looks at the most relevant singular values rather than the total set to improve the results. This does cause the optimization to no longer be convex however. Improvements were made in [48] to reduce the computational complexity of the problem. The problem statement can also be generalized to any basis of desire [49]. Matrix completion can also be applied to higher rank matrices, under the assumption that the matrix is comprised of

several independent or overlapping lower rank matrices [50]. This would be applicable in more complex systems with a varying degree of correlation between the variables.

There has been work done in an attempt to provide conditions on the number of available data points such that the matrix completion algorithm returns an accurate estimate [35]. From this, it is seen that the number of observations needed is proportional to the rank and size of the matrix.

Due to the nature of the equality constraint, formulation (4.3) is highly susceptible to noise. To alleviate this, [51] proposed a robust algorithm to handle noisy measurements. The algorithm modifies the equality constraint in (4.3) to

$$\|X_\Omega - M_\Omega\|_F \leq \delta \tag{4.5}$$

where $\|X\|_F$ is the Frobenius norm of X which is defined as

$$\|X\|_F = \sqrt{\sum_{i=1}^{m}\sum_{j=1}^{n}|X_{i,j}|^2}. \tag{4.6}$$

The accuracy of the estimations is highly correlated to the value of δ selected. Since the value of δ corresponds to the amount of noise in the measurements, the accuracy of the estimation naturally increases when δ becomes closer to zero. Bad data can be somewhat dealt with through the exclusion of data points when they are significantly different than what should be reasonable, which will require accurate bad data detection. Otherwise, if there are enough measurements available the algorithm is robust against few bad data points.

4.2 Low Observability Voltage Estimation

In this section, we propose a new matrix-completion-based approach for voltage estimation under low observability. The overarching idea of our approach is to augment the standard matrix completion problem presented in Section 4.1 with power-flow constraints in order to

obtain better accuracy with less data required.

4.2.1 Power System Model

For brevity, we consider a balanced network with a single slack bus and N, PQ buses. Let $\mathcal{N} = \{1, \ldots, N\}$ denote the set of the PQ buses, and $\mathcal{L} \subseteq \mathcal{N} \times \mathcal{N}$ denote the set of distribution lines. We note that the formulation proposed in this paper can be easily extended to the general multiphase setting with both wye and delta connections, as proposed, e.g., in [52].

4.2.2 Matrix Set-Up

The selection of proper matrix variables is paramount to accurate matrix completion results. Since the objective of the estimation is to determine the voltages at each bus, parameters which have a correlation to the voltage must be selected to obtain the most accurate results.

In order to allow for the use of the largest number and variety of variables, we set up the matrix in terms of system connection lines rather than buses. In this way, each row of the matrix represents one line in the system, and each column represents one variable. The matrix will need to be modified as the topology of the system changes, but this is done simply with the inclusion and removal of rows within the matrix.

The resultant matrix columns then are selected as: the real and reactive voltage from the source bus of the line, the total real and reactive power entering the line source bus from all sources (generators and lines), the real and reactive current flowing through the line, the power flowing through the line, the load at the source bus, and the voltage magnitude at the source bus. Formally, for every line $(f, t) \in \mathcal{L}$, the corresponding row in the matrix M is given by

$$[Re(V_f), Im(V_f), P_{in_f}, Q_{in_f}, Re(I_{f,t}), Im(I_{f,t}), P_{flow_{f,t}},$$
$$Q_{flow_{f,t}}, P_{load_f}, Q_{load_f}, |V_f|].$$

We note that the proposed algorithm is not limited to the variables selected above. In fact,

any variables which have a correlation with voltage can be used to supplement and improve the results.

4.2.3 Power Flow Constraints

We next formulate several corresponding constraints to be included in the original formulation. First, since the objective matrix contains both the voltages at each bus and the current flowing between buses, the power flow constraints can be introduced to the optimization in the form of the following linear equality constraint:

$$(V_f - V_t)Y_{ft} = I_{ft},\ \forall (f,t) \in \mathcal{L}. \tag{4.7}$$

However, the inclusion of this constraint might result in the infeasibility of the problem. To increase the robustness of the algorithm against varying system conditions and measurement noise, the power flow equality constraints are relaxed and bounded by a tolerance. The new constraint then becomes

$$-\epsilon_{f,t} \leq (V_f - V_t)Y_{ft} - I_{ft} \leq \epsilon_{f,t},\ \forall (f,t) \in \mathcal{L}, \tag{4.8}$$

where $\epsilon_{f,t}$ is the error tolerance for line $(f,t) \in \mathcal{L}$.

Additionally, it is a natural requirement for there to be net zero power at each bus. Thus, the power flowing into the bus must be equal to the power consumed at the bus plus the power leaving the bus. This can be formulated as

$$\begin{aligned} P_{in_f} - \sum_{t \in \mathcal{N}} P_{flow_{f,t}} - P_{load_f} = 0,\ \forall f \in \mathcal{N}, \\ Q_{in_f} - \sum_{t \in \mathcal{N}} Q_{flow_{f,t}} - Q_{load_f} = 0,\ \forall f \in \mathcal{N}. \end{aligned} \tag{4.9}$$

Similarly to constraint (4.8), we relax these equality constraints as follows:

$$\begin{aligned} -\tau_f \leq P_{in_f} - \sum_{t\in\mathcal{N}} P_{flow_{f,t}} - P_{load_f} \leq \tau_f,\ \forall f \in \mathcal{N} \\ -\tau_f \leq Q_{in_f} - \sum_{t\in\mathcal{N}} Q_{flow_{f,t}} - Q_{load_f} \leq \tau_f,\ \forall f \in \mathcal{N} \end{aligned} \tag{4.10}$$

where τ_f is the error tolerance for bus $f \in \mathcal{N}$.

Feasibility can then be ensured by selecting tolerance values which create a feasible problem. However, since the accuracy of the resultant estimation is dependent on the tolerance being minimal, the values used need to be included in the optimization objective. Therefore, augmenting the original matrix completion problem (4.3), (4.5) with the power flow constraints, results in the following optimization problem:

$$\min_{X\in\mathbb{R}^{n_1\times n_2},\{\epsilon_{f,t}\},\{\tau_f\}} \|X\|_* + w_1 \sum_{(f,t)\in\mathcal{L}} \epsilon_{f,t} + w_2 \sum_{f\in\mathcal{N}} \tau_f \tag{4.11a}$$

$$\text{s.t.}\ \ \|X_\Omega - M_\Omega\|_F \leq \delta \tag{4.11b}$$

$$(4.8),\ (4.10) \tag{4.11c}$$

$$\epsilon_{f,t} \geq 0,\ \forall (f,t) \in \mathcal{L} \tag{4.11d}$$

$$\tau_f \geq 0,\ \forall f \in \mathcal{N}, \tag{4.11e}$$

where $w_1, w_2 > 0$ are weighting parameters that are used to tune the trade-off between the accuracy of estimation and slackness of the optimization problem; $n_1 := |\mathcal{L}|$ is the number of lines in the network; and n_2 is the number of variables used for estimation. Observe that, since the measurements are in rectangular coordinates, (4.11) is a convex optimization problem and hence can be solved efficiently.

We note that, when the measurements of voltage magnitudes and/or power injections are available, formulation (4.11) can be augmented with additional constraints to capture the dependence between these variables. In the next two subsections, we propose two different ways to include these constraints: one that is applicable to only radial distribution networks and another one that is applicable to general systems.

Radial Networks

The LinDistFlow approximation for power-flow equations [53] can be used under the assumption that the network is radial and of low power, as found in distribution networks. The LinDistFlow voltage approximation is given by

$$|V_t| = |V_f| - (r_{f,t}P_{flow_{f,t}} + x_{f,t}Q_{flow_{f,t}})/|V_0| \tag{4.12}$$

where V_0 is the voltage magnitude at the feeder head, and $r_{f,t}$ and $x_{f,t}$ are the resistance and reactance of line (f,t), respectively. This constraint is once again relaxed and added to the optimization problem, resulting in:

$$\min_{X\in\mathbb{R}^{n_1\times n_2},\{\epsilon_{f,t}\},\{\tau_f\}} \|X\|_* + w_1 \sum_{(f,t)\in\mathcal{L}} \epsilon_{f,t} + w_2 \sum_{f\in\mathcal{N}} \tau_f + w_3 \sum_{(f,t)\in\mathcal{L}} \gamma_{f,t} \tag{4.13a}$$

$$\text{s.t. } (4.11\text{b}) - (4.11\text{e}) \tag{4.13b}$$

$$\Big||V_t| - |V_f| + (r_{f,t}P_{flow_{f,t}} + x_{f,t}Q_{flow_{f,t}})/|V_0|\Big| \leq \gamma_{f,t},\ \forall (f,t)\in\mathcal{L} \tag{4.13c}$$

$$\gamma_{f,t} \geq 0,\ \forall (f,t)\in\mathcal{L} \tag{4.13d}$$

General Networks

The inclusion of the voltage magnitude constraints for general networks is slightly more involved. The mathematics for deriving the convex constraints between the voltage and the remaining quantities can be found in, e.g., [54]. Given a reference bus, define $\tilde{v}$ as the array of voltage phasors at the remaining buses and $|\tilde{v}|$ as the voltage magnitudes for the remaining buses. Additionally define s^Y as the subsequent vectors of real and reactive powers($s^Y = ((p^Y)^T, (q^Y)^T)$) for Y-connected buses, and s^Δ as the vectors of real and reactive power for delta-connected buses. Split the admittance matrix, such that the reference bus

is a separate matrix, as seen below.

$$Y = \begin{bmatrix} Y_{00} & Y_{0L} \\ Y_{L0} & Y_{LL} \end{bmatrix}$$

Finally, define H as the diagonal matrix of Γ, where

$$\Gamma = \begin{bmatrix} 1 & -1 & 0 \\ 0 & 1 & -1 \\ -1 & 0 & 1 \end{bmatrix}$$

Given an initial solution of $\hat{v}$,$\hat{S^Y}$, and $\hat{s^\Delta}$. Construct matrices such that

$$\begin{aligned} M^Y &= (Y_{LL}^{-1} diag(\hat{v})^{-1}, -jY_{LL}^{-1} diag(\hat{v})^{-1}) \\ M^\Delta &= (Y_{LL}^{-1} H^T diag(H\hat{v})^{-1}, -jY_{LL}^{-1} H^T diag(H\hat{v})^{-1}) \end{aligned} \tag{4.14}$$

Additionally, create the vectors and matries of

$$\begin{aligned} w &= -Y_{LL}^{-1} Y_{L0} v_0 \\ W &= diag(w) \end{aligned} \tag{4.15}$$

Combining to form

$$\begin{aligned} K^Y &= |W| Re W^{-1} M^Y \\ K^\Delta &= |W| Re W^{-1} M^\Delta \end{aligned} \tag{4.16}$$

In particular, linear approximations of both the voltage phasor and voltage magnitude can be defined as

$$\begin{aligned} v &\approx Mx + w \\ |v| &\approx Kx + |w|, \end{aligned} \tag{4.17}$$

where $v \in \mathbb{C}^N$ and $|v| \in \mathbb{R}^N$ are, respectively, the voltage phasors and magnitudes at all buses; $x \in \mathbb{R}^{2N}$ is the vector of active and reactive power injections at all buses; and the matrices $M \in \mathbb{C}^{N\times 2N}$, $K \in \mathbb{R}^{N\times 2N}$ and vectors $w \in \mathbb{C}^N$ and $|w| \in \mathbb{R}^N$ can be computed as in [52, 54].

Considering these approximation as constraints, it is required once again to relax them, which yields the following optimization problem for general networks:

$$\min_{X\in\mathbb{R}^{n_1\times n_2},\{\epsilon_{f,t}\},\{\tau_f\}} \|X\|_* + w_1 \sum_{(f,t)\in\mathcal{L}} \epsilon_{f,t} + w_2 \sum_{f\in\mathcal{N}} \tau_f + w_3\gamma + w_4\alpha \tag{4.18a}$$

$$\text{s.t. } (4.11b) - (4.11e) \tag{4.18b}$$

$$\|v - Mx - w\|_\infty \leq \gamma \tag{4.18c}$$

$$\||v| - Kx - |w|\|_\infty \leq \alpha. \tag{4.18d}$$

4.3 Simulation and Results

Simulations were performed in both radial and mesh networks to show the viability of the algorithm for both cases.

4.3.1 Radial Network Results

The test case for the radial network is the IEEE standard 33 bus system as shown in Figure 4.1.

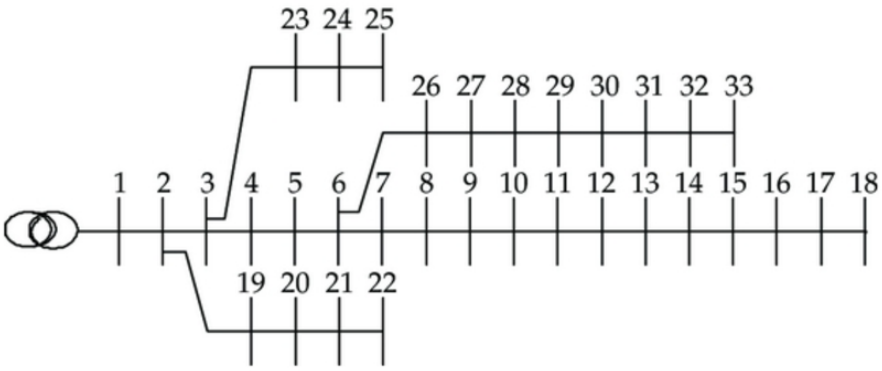

Figure 4.1: IEEE Standard 33 Bus System

Unless otherwise stated, all simulations are run under the assumption of a single voltage phasor measurement and 50% of the remaining quantities obtained through uniform random sampling for each case. In radial networks with low number of voltage phasor measurements, the voltage magnitude estimations need to be scaled to be within the proper range. Without voltage scaling, the magnitude estimations will still follow the proper trend. However, since the other quantities in the matrix can vary much more significantly, the estimations will be outside of the correct voltage range. This scaling can be done through

$$V_{new} = V_{min} + (V_{max} - V_{min})(\frac{V_{old} - V_{est_{max}}}{V_{est_{max}} - V_{est_{min}}}). \tag{4.19}$$

This is required in radial systems with only two or fewer voltage phasor measurements. As the number increases beyond this, voltage scaling no longer becomes necessary. The magnitude measurement can be obtained from either the phasor measurement or the pure measurement. However, it is still required to have both the maximum and minimum voltage magnitude to obtain the optimal results when there are not enough phasor measurements.

Figure 4.2 shows the results of applying the matrix completion formulation (4.13) to the entire IEEE 33 bus radial system.

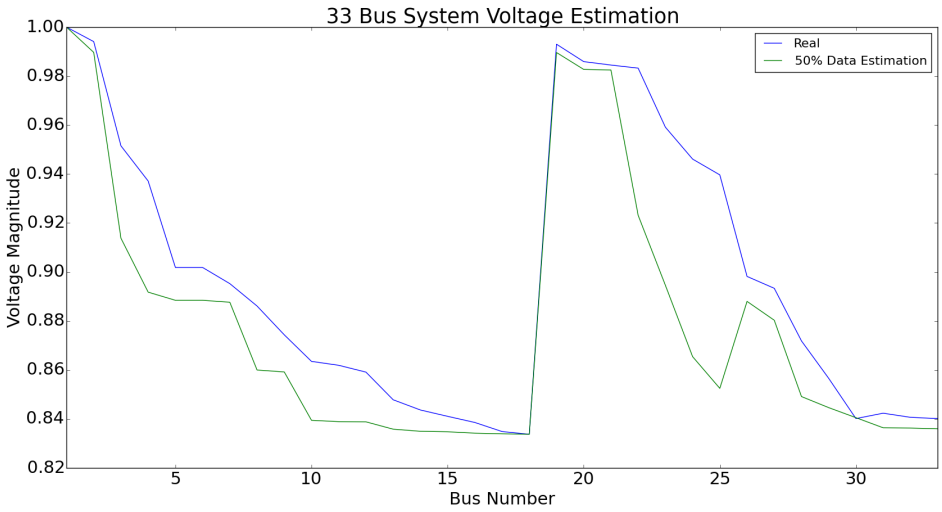

Figure 4.2: Voltage Estimation of Radial Network

It can be seen that the estimations follow the trend very well. There are occasional large deviations from the true value, due to the algorithm being highly dependent on which data was available when making the estimation. These results were produced under the assumption that the data available was uniformly randomly sampled from the complete data set, which is not necessarily the case for real systems.

Figure 4.3 shows the impact of observability on the mean absolute percentage error(MAPE) of the estimations.

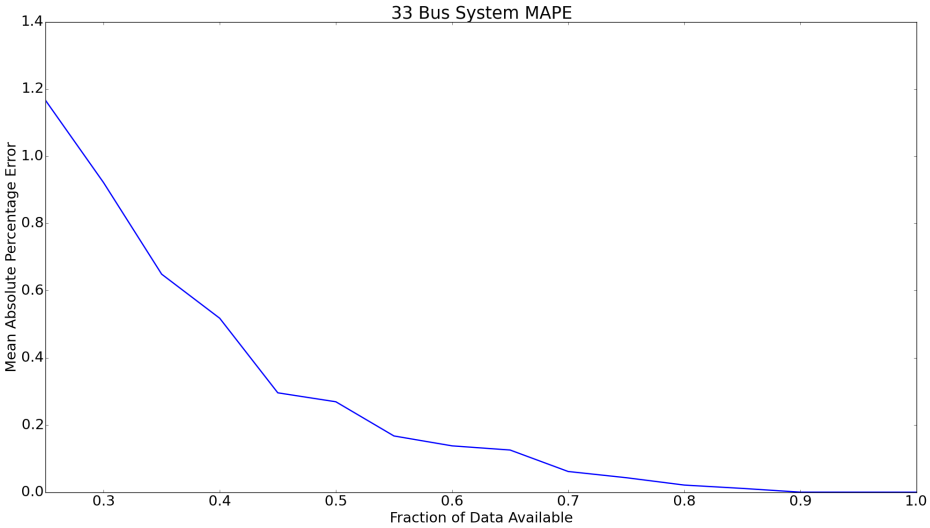

Figure 4.3: MAPE as Observability Increases

The results in Figure 4.4 show that the approach is applicable for angle estimations as well, with a slight increase on the noise of the estimations. Additionally, the amount of voltage phasor measurements required to obtain accurate results is increased when estimating angle values. The plot in Figure 4.4 was obtained with a voltage phasor measurement at Bus 1 and the ending Bus of all branches(18,22,25,33) in the IEEE 33 Bus system.

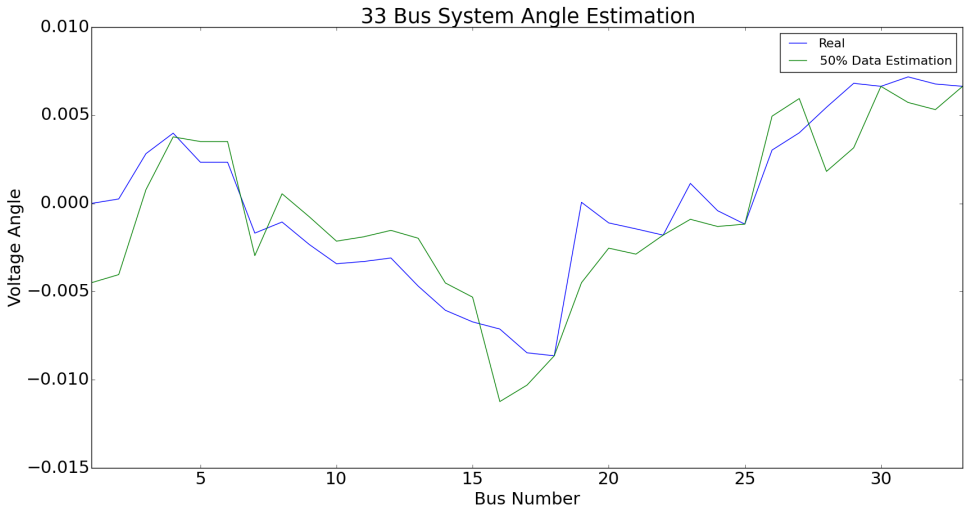

Figure 4.4: Voltage Angle Estimation of Radial Network

While this approach results in accurate estimations, no algorithm would be acceptable without being able to handle error on the measurements. To show that this procedure is robust against system errors, varying amounts of noise were added to the data. The noise was set to follow a normal distribution centered around the actual value with a standard deviation of a set percentage of the actual value. All plots were run using 50 percent data availability, while only a single voltage phasor measurement was used at bus 1. Additionally, the missing elements were the same for each case such that the only difference in estimations was the error. From Figure, 4.5 it can be seen that while measurement errors do have some impact on the resultant estimation, the availability of data has a much more significant impact.

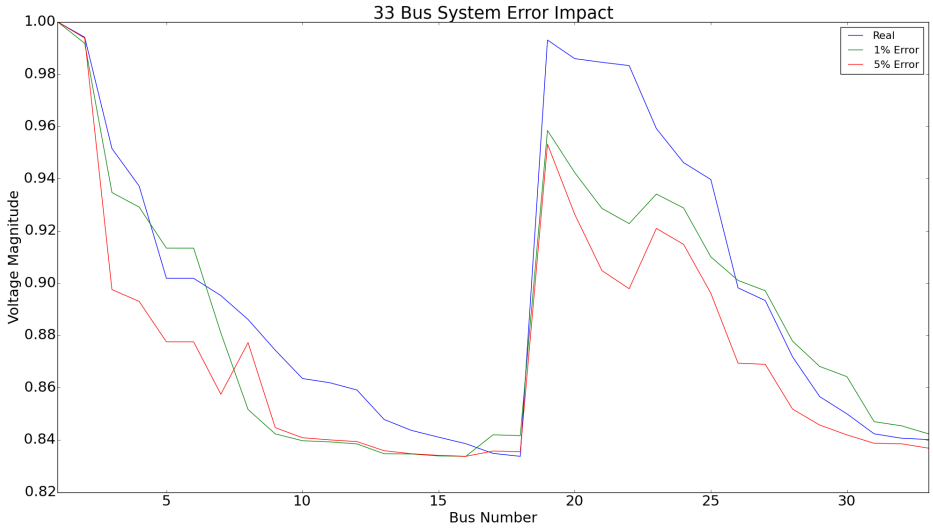

Figure 4.5: Impact of Measurement Errors

The results thus far have been done under the assumption of only one single voltage phasor measurement to show the accuracy under minimal investment into new sensors in the system. However, as the number of voltage phasor measurements increases, the accuracy of the estimations increases significantly. Figure 4.6 shows how the accuracies of the estimation will improve as the number of voltage phasor measurements increase.

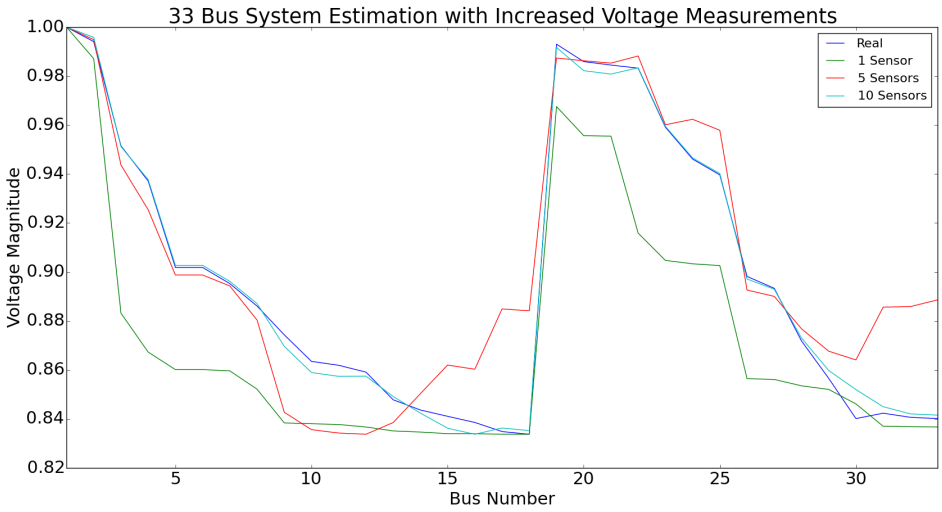

Figure 4.6: Impact of Number of Phasor Measurements in Radial Network

One item of note that was not included in these results is that new voltage phasor measurement devices installed into the grid, typically in the form of synchrophasors or micro-synchrophasors, have the capability of measuring current as well. Thus, the increase in accuracy due to increasing the number of sensors will be much more significant than the results show.

Another fact that has a significant impact on the accuracy of results is the issue of where new voltage phasor measurement devices are installed. Simply increasing the number of voltage phasor measurements may have a positive impact on the accuracy of the estimations, but the algorithm can be improved optimally when considering where the new voltage phasor measurements should be located. Figure 4.7 shows the difference in estimation accuracies in the IEEE 33 Bus system when there are five voltage phasor measurements at the first five buses versus when they are at bus one and at the ending bus of each branch. The results shown are without the voltage scaling that was done in the previous radial system results to highlight the significance on placing the measurement devices properly.

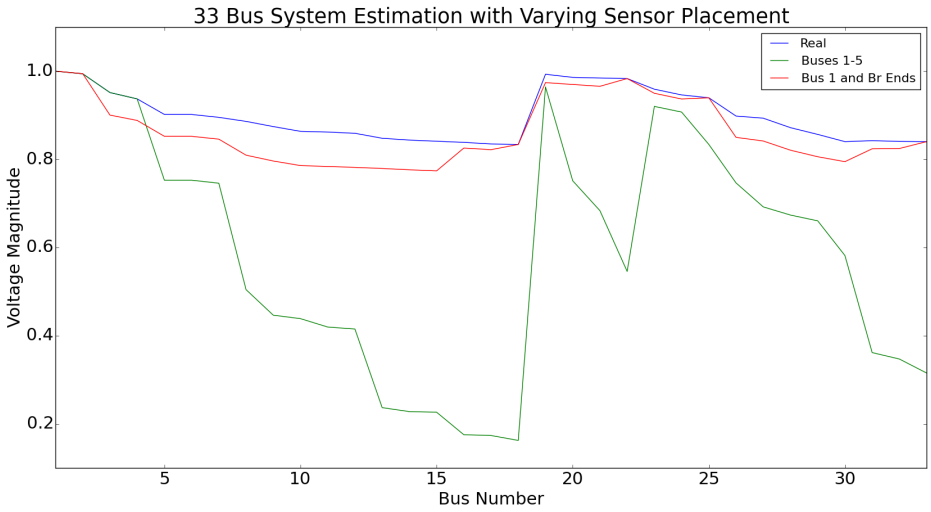

Figure 4.7: Impact of Phasor Measurement Device Placement

While the estimations using devices at the first five buses can identify the overall trend of the voltages properly, it is much more susceptible to noise and missing data. Additionally, it can be see that when the measurement devices are more spread out, the accuracy is much higher and does not necessarily require, yet would be aided by, voltage range scaling.

Overall, using matrix completion to estimation voltages at all locations will produce accurate results under the correct circumstances. There are several conditions that will cause inaccurate results, and the approach has significant room for improvement. However, the results obtained with minimal available data are very promising.

4.3.2 Mesh Network Results

The same tests were also performed on a mesh network. The test case for the mesh network is the IEEE standard 39 bus system as shown in Figure 4.8.

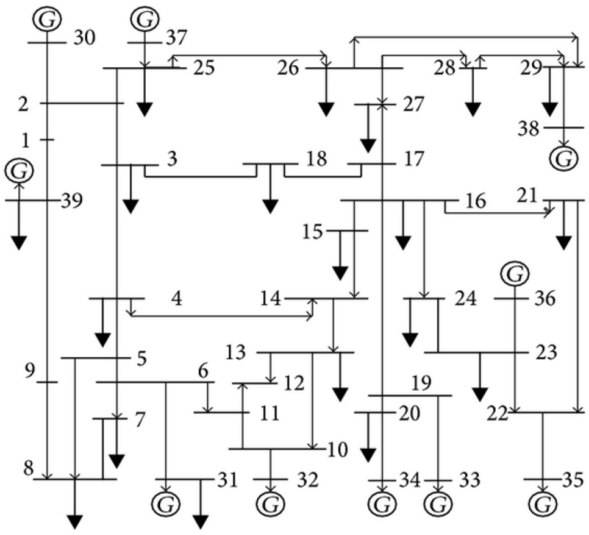

Figure 4.8: IEEE Standard 39 Bus System

Figures 4.9 and 4.10 shows the application of the algorithm to a mesh network. While the algorithm does provide accurate results for the mesh network, there is a considerable increase in the computational complexity of the problem.

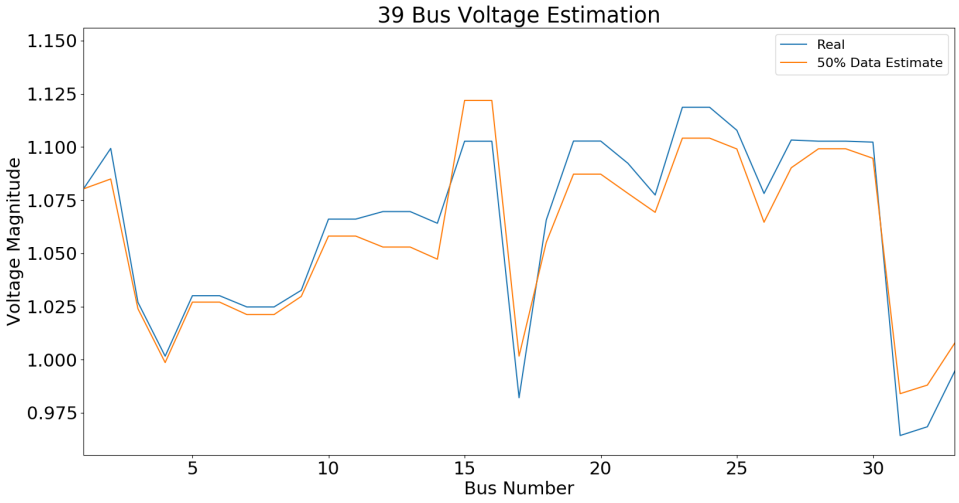

Figure 4.9: Voltage Estimation of Mesh Network

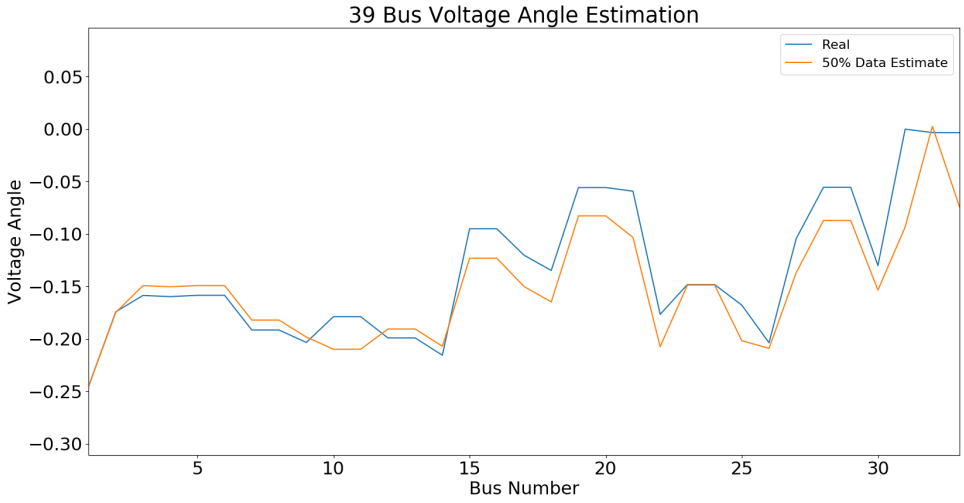

Figure 4.10: Voltage Angle Estimation of Mesh Network

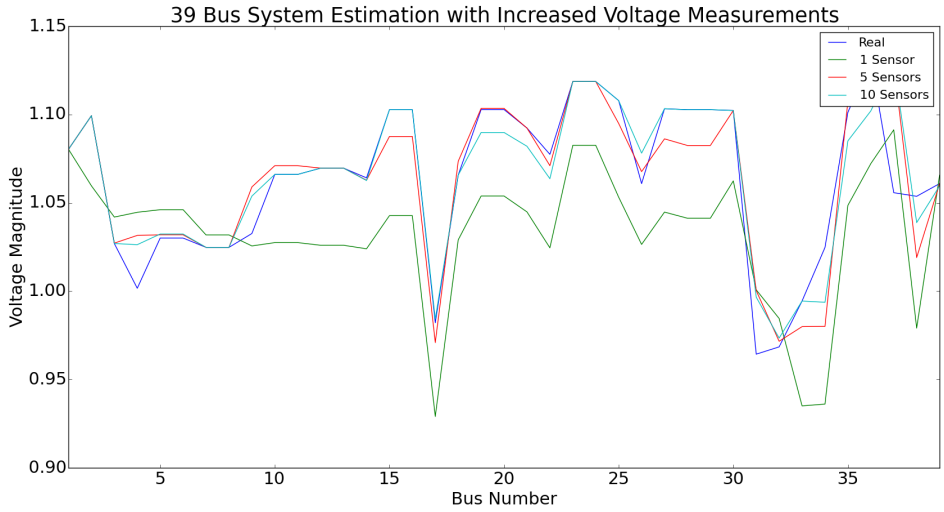

Figure 4.11: Impact of Number of Phasor Measurements in Mesh Network

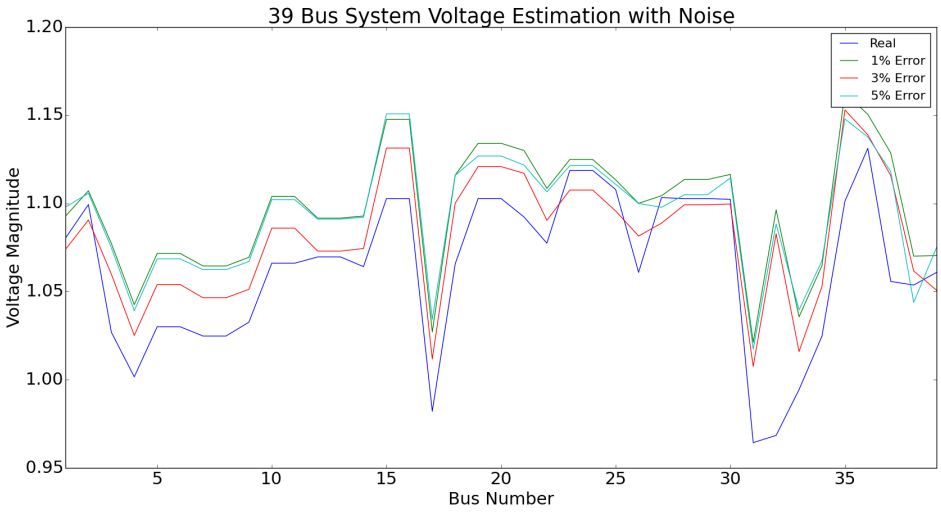

Figure 4.12: Impact of Measurement Errors in Mesh Network

4.4 Model-Free Voltage Estimation

The original matrix completion algorithm can be applied as is, without including the additional power system constraints, to the formed matrix for radial systems to estimate voltages with relative accuracy. The advantage of doing this is in the fact that no parameters of the network model are required to obtain results. This becomes beneficial when there is no information available about the model or when the information has potential inaccuracies. However, as this requires a very strong correlation between variables within the matrix and a very low rank, it is only possible for radial networks and is highly susceptible to the quantities available for completion.

Additional steps are required in order to obtain accurate results without the use of a model. First, the system needs to be split into several clusters which are equivalent to the branches of the system. To obtain accurate results, a separate matrix needs to be constructed for each branch.

One draw back for the model-free approach is that the voltage scaling previously discussed

is required for all cases following equation (4.19). The results of the matrix estimation when all matrix elements except voltage are known, can be seen in Figure 4.13.

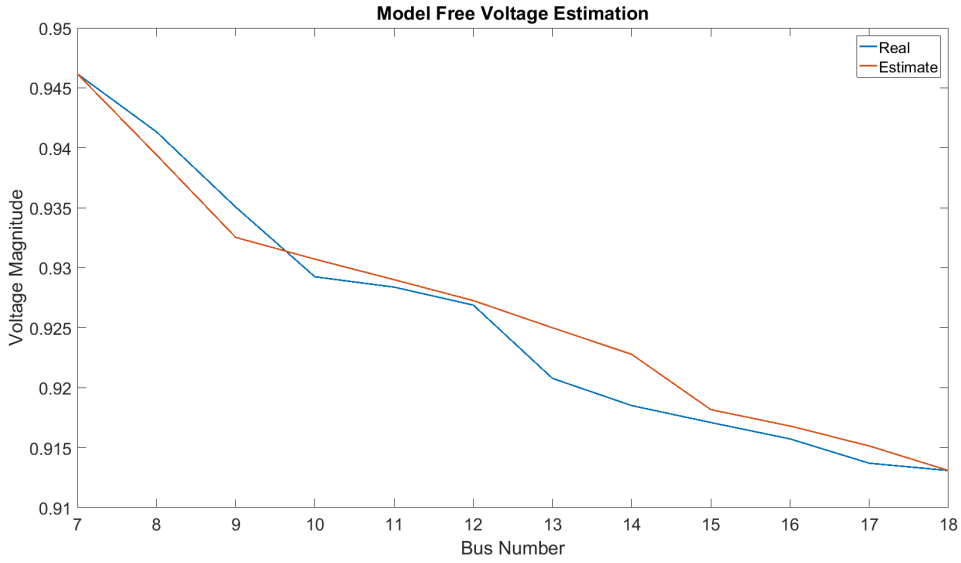

Figure 4.13: Voltage Estimation with No Missing Data

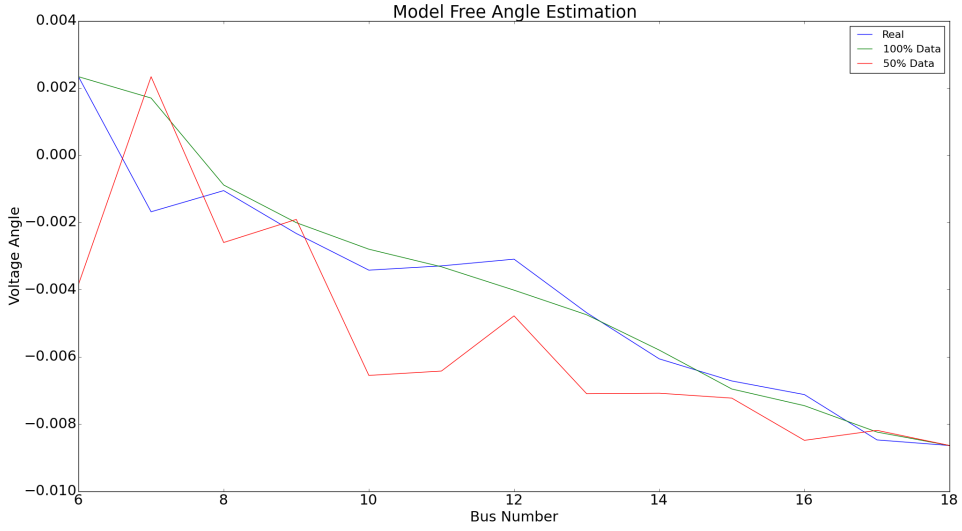

Figure 4.14: Angle Estimation with Missing Data

Additionally, this procedure will work for systems with slight PV injections and more im-

portantly, when the data is incomplete as can be seen in Figure 4.15.

Figure 4.15: Voltage Estimation with Missing Data

The plot shows that the estimations follow the trend relatively accurately for most estimations. The PV injection is at Bus 14. The accuracy of each estimation depends entirely on which data was available at the respective bus. In Figure 4.15, this can be seen in the few estimations at the 50 % data available which are significantly different from the trend, while some are extremely similar.

It can also be shown that as the fraction of known elements within the matrix increases, the accuracy of the estimations will increase. This can be seen in Figure 4.16, which shows that mean absolute percentage error of the voltage estimates as the number of known elements increases. Even with averaging multiple runs, it can be seen that the estimations will vary significantly depending on which data is available during the estimation.

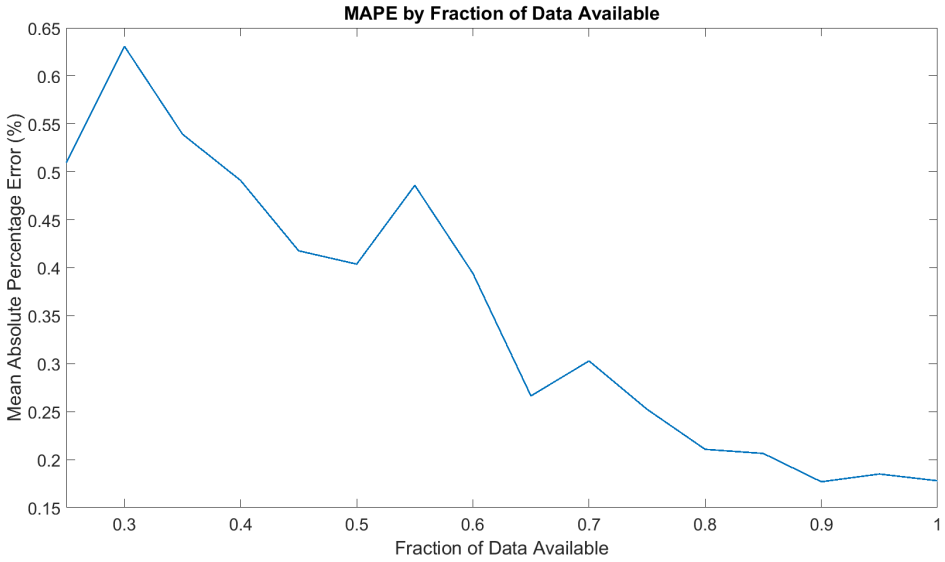

Figure 4.16: MAPE as Observability Increases

It should be noted that the inclusion of significant PV or power injections at a node creates a complication in this procedure. The algorithm will accurately estimate up to the node which contains the PV, but will have significant errors afterwards. This is due to the assumption made of each branch having an individual matrix for completion, as stated previously. When significant PV is present at a node, this essentially causes the branch to be split into two separate branches at the node, since branches are defined by the flow of the current. If the PV injection is large enough such that current flows in both directions out the node, separate matrices need to be made for each side of the node.

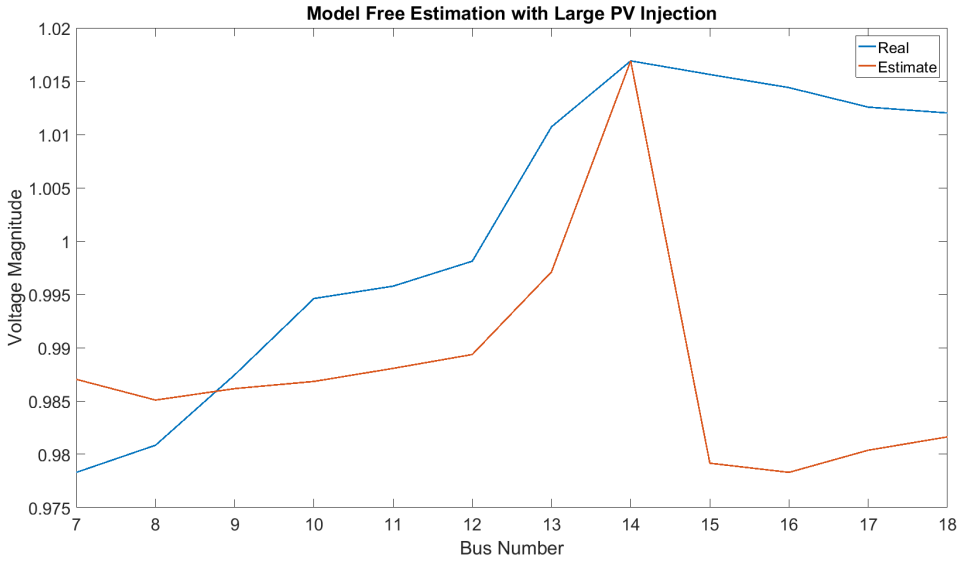

Figure 4.17: High PV Injection Voltage Estimation

4.5 Comparison to Traditional Methods

While low observability cases are the goal of this approach, the purpose of full observability state estimation is to eliminate errors and noise in the measurements. Full observability can be defined as the case when the measurement Jacobian matrix has full rank. It can be shown that this approach is also capable of properly dealing with these measurement errors when the δ parameter is properly tuned as seen in Figure 4.18. The results from Figure 4.18 were obtained with the constrained matrix completion algorithm under full observability and noisy measurements. This allows for the completion of state estimation with results comparable to traditional techniques, such as WLS, in systems that have sufficient observability, as well as the estimation of states in systems that have low observability.

Additionally, as seen in Figure 4.19, the accuracy of matrix completion is better than that of WLS when observability decreases. Since traditional techniques, such as WLS, require full observability when applied to the power systems, in order to apply them to cases with

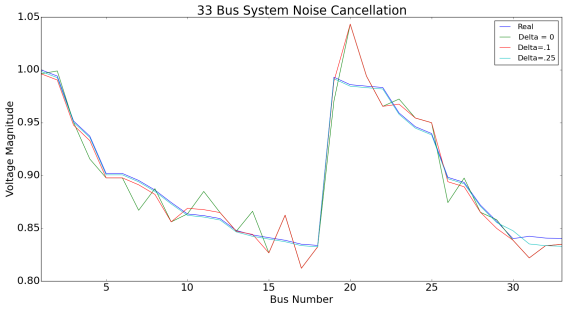

Figure 4.18: Impact of δ Value

reduced observability pseudo-measurements are used. Pseudo-measurements are values that are chosen, typically based upon historical profiles of the system. It has been shown that these values can be highly inaccurate. For the results seen in Figure 4.19, a 10% error was used for the pseudo-measurements.

For both algorithms, WLS and matrix completion, the estimation was performed as the number of measured locations decreased until 50% observability was reached. When the removal of a certain location results in the reduction of observability(the rank of the observability Jacobian matrix decreased), those measurements were replaced with pseudo-measurements. This process was repeated numerous times, and the results averaged to produce the results in Figure 4.19.

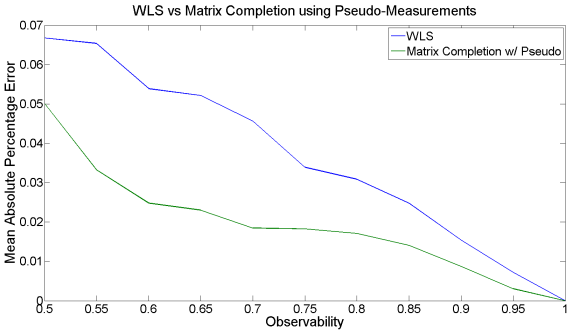

Figure 4.19: MAPE of WLS vs Matrix Completion as Observability Increases

This validates that when comparing the matrix completion algorithm to WLS under the same scenario, the results from matrix completion are more accurate.

Chapter 5

Conclusions

The ability to perform power system stability assessments relies upon the availability of certain key parameters. The work presented in this dissertation details method in which to estimate three of these parameters: Inertia, Topology, and Voltage. The major contributions of this work are:

- The creation of a procedure to be able to estimate power system inertia values during steady-state system conditions using a machine learning based approach
- A new substation topology estimation algorithm that is able to produce results solely through the use of synchrophasor data, without requiring access to breaker status telemetry
- The improvement of voltage phasor estimation accuracy in systems with low observability through the use of a new matrix completion based algorithm

5.1 Inertia Estimation Conclusions

Being able to accurately estimate the inertia in a system is becoming increasingly important. Power supplied by renewable energy sources will continue to increase and steps need to be taken in order to ensure system stability. The importance of the inertia parameter in a system is well known, however techniques to obtain this value are currently insufficient. Current techniques rely upon fault conditions to occur before values can be estimated. Since these events should be avoided and are infrequent, these techniques are not ideal.

This procedure detailed in this work is able to estimate regional and system inertia values under steady state conditions. The method makes use of modal information obtained through the use of empirical orthogonal functions on frequency values which can be obtained from synchrophasors. The modal information is used in a neural network to estimate the inertia values at individual buses as well as regional and system values.

While the purpose of this research was to use modal information to estimate system values, there are other values which may be beneficial to use in conjunction with the modal information in an attempt to improve the accuracy of the results. The inclusion of these parameters, such as voltage, frequency or phase angle, may have a positive impact on the ability of the neural network to correctly estimate inertia values for the individual buses. The goal moving forward is to improve the accuracy of the results by including these parameters in the neural network; however, as it is now, the method is viable if the aim is to estimate either the regional or system inertia values.

5.2 Topology Estimation Conclusions

Topology estimation techniques are very limited in their current scope, yet the knowledge of a power systems topology has a tremendous impact on the operations of a grid and is paramount to optimal grid operations. The wide availability of synchrophasor data allows

for the estimation of a power systems topology through the use of voltage phasor deviations. As nodes become disconnected, the difference between their voltage phasor values will increase. If the difference is above a determined threshold, it can be said that the nodes are disconnected. This threshold can be determined through an empirical approach which measures the voltage difference across disconnected nodes for all possible configurations of the system. The threshold is then obtained from this data such that it is statistically significant while remaining a realistic value.

Through the use of this determined threshold, the breaker statuses can be inferred. In this way, the topology of the substation can be reconstructed. The results show that this procedure is highly accurate when synchrophasor measurements adhere to the required standard measurement errors. As measurement errors increase, the estimation accuracy drops but can be improved to a certain extent through the modification of the voltage phasor deviation threshold.

With the ability to infer the topology, or a subset of the topology, of a substation, many analytics are more effective and the overall operation of the power grid improves drastically.

5.3 State Estimation Conclusions

The continued increase of deployment of distributed generation in the distribution network has caused the need for accurate knowledge of the current state of the network. Unfortunately, the vast size of the distribution network causes the instillation of the required number of measurements for traditional state estimation to be infeasible. Thus the need for low observability state estimators has become apparent.

The approach detailed in this paper makes use of auxiliary measurements in the form of smart meters, PV inverters, etc., to supplement the information about the system for the completion of state estimation. These measurements are then applied to a matrix completion algorithm which estimates the unknown quantities. With a focus on the voltage phasor, it is

shown that even under scenarios with very low observability, the voltage phasor is obtainable with relative accuracy.

The major contributions of this approach is the ability of the algorithm to make use of any type of measurement, not just voltage phasors, current phasors, and power measurements. Whatever measurements are present in the system at a given time, including wind speed, solar irradiance, measurements from inverters or other smart devices, etc., can be included to obtain results where previously state estimation could not have been done. Thus, without the huge burden of installing new measurement devices, it is still possible to perform state estimation with accurate results.

Bibliography

[1] P. Kundur, J. Paserba, V. Ajjarapu, G. Andersson, A. Bose, C. Canizares, N. Hatziargyriou, D. Hill, A. Stankovic, C. Taylor, T. V. Cutsem, and V. Vittal, "Definition and classification of power system stability ieee/cigre joint task force on stability terms and definitions," *IEEE Transactions on Power Systems*, vol. 19, no. 3, pp. 1387–1401, Aug 2004.

[2] A. Meanovi, U. Mnz, and C. Heyde, "Comparison of h, h2, and pole optimization for power system oscillation damping with remote renewable generation," *IFAC-PapersOnLine*, vol. 49, no. 27, pp. 103 – 108, 2016, iFAC Workshop on Control of Transmission and Distribution Smart Grids CTDSG 2016. [Online]. Available: http://www.sciencedirect.com/science/article/pii/S2405896316323461

[3] B. Kameshwar Poolla, S. Bolognani, and F. Dorfler, "Optimal Placement of Virtual Inertia in Power Grids," *ArXiv e-prints*, Oct. 2015.

[4] A. Ulbig, T. S. Borsche, and G. Andersson, "Impact of Low Rotational Inertia on Power System Stability and Operation," *ArXiv e-prints*, Dec. 2013.

[5] A. Ulbig, T. S. Borsche, and G. Andersson, "Analyzing rotational inertia, grid topology and their role for power system stability," *IFAC-PapersOnLine*, vol. 48, no. 30, pp. 541 – 547, 2015, 9th IFAC Symposium on Control of Power and Energy Systems CPES 2015. [Online]. Available: http://www.sciencedirect.com/science/article/pii/S2405896315030785

[6] P. M. Ashton, C. S. Saunders, G. A. Taylor, A. M. Carter, and M. E. Bradley, "Inertia estimation of the gb power system using synchrophasor measurements," *IEEE Transactions on Power Systems*, vol. 30, no. 2, pp. 701–709, March 2015.

[7] T. Inoue, H. Taniguchi, Y. Ikeguchi, and K. Yoshida, "Estimation of power system inertia constant and capacity of spinning-reserve support generators using measured frequency transients," *IEEE Transactions on Power Systems*, vol. 12, no. 1, pp. 136–143, Feb 1997.

[8] S. Guo, S. Norris, and J. Bialek, "Adaptive parameter estimation of power system dynamic model using modal information," *IEEE Transactions on Power Systems*, vol. 29, no. 6, pp. 2854–2861, Nov 2014.

[9] M. Bostanci, J. Koplowitz, and C. W. Taylor, "Identification of power system load dynamics using artificial neural networks," *IEEE Transactions on Power Systems*, vol. 12, no. 4, pp. 1468–1473, Nov 1997.

[10] L. Xiao-fei and S. Li-qun, "Power system load forecasting by improved principal component analysis and neural network," in *2016 IEEE International Conference on High Voltage Engineering and Application (ICHVE)*, Sept 2016, pp. 1–4.

[11] N. Vempati, C. Silva, O. Alsac, and B. Stott, "Topology estimation," in *IEEE Power Engineering Society General Meeting, 2005*, June 2005, pp. 806–810 Vol. 1.

[12] A. M. Sasson, S. T. Ehrmann, P. Lynch, and L. S. V. Slyck, "Automatic power system network topology determination," *IEEE Transactions on Power Apparatus and Systems*, vol. PAS-92, no. 2, pp. 610–618, March 1973.

[13] P. D. Yehsakul and I. Dabbaghchi, "A topology-based algorithm for tracking network connectivity," *IEEE Transactions on Power Systems*, vol. 10, no. 1, pp. 339–346, Feb 1995.

[14] M. Farrokhabadi and L. Vanfretti, "Phasor-assisted automated topology processing for state estimators," in *2013 IEEE Electrical Power Energy Conference*, Aug 2013, pp. 1–8.

[15] M. Prais and A. Bose, "A topology processor that tracks network modifications," *IEEE Transactions on Power Systems*, vol. 3, no. 3, pp. 992–998, Aug 1988.

[16] M. Zhou, V. A. Centeno, J. S. Thorp, and A. G. Phadke, "An alternative for including phasor measurements in state estimators," *IEEE Transactions on Power Systems*, vol. 21, no. 4, pp. 1930–1937, Nov 2006.

[17] K. D. Jones, J. S. Thorp, and R. M. Gardner, "Three-phase linear state estimation using phasor measurements," in *2013 IEEE Power Energy Society General Meeting*, July 2013, pp. 1–5.

[18] C. Qian, Z. Wang, and J. Zhang, "A new algorithm of topology analysis based on pmu information," in *2010 5th International Conference on Critical Infrastructure (CRIS)*, Sept 2010, pp. 1–5.

[19] H. Mori and S. Saito, "A power system state estimation technique in consideration of network topology," in *2006 IEEE International Conference on Systems, Man and Cybernetics*, vol. 3, Oct 2006, pp. 1837–1842.

[20] L. Mili, G. Steeno, F. Dobraca, and D. French, "A robust estimation method for topology error identification," *IEEE Transactions on Power Systems*, vol. 14, no. 4, pp. 1469–1476, Nov 1999.

[21] A. S. Costa and F. Vieira, "Topology error identification through orthogonal estimation methods and hypothesis testing [power systems]," in *2001 IEEE Porto Power Tech Proceedings (Cat. No.01EX502)*, vol. 3, 2001, pp. 6 pp. vol.3–.

[22] A. Abur and A. G. Exposito, *Power System State Estimation: Theory and Implementation*. Abingdon: Dekker, 2004. [Online]. Available: http://cds.cern.ch/record/994935

[23] M. E. Baran, "Challenges in state estimation on distribution systems," in *2001 Power Engineering Society Summer Meeting. Conference Proceedings (Cat. No.01CH37262)*, vol. 1, July 2001, pp. 429–433 vol.1.

[24] M. Baruki, M. Vukobratovi, D. Masle, D. Bulji, and . Herderi, "The evolutionary optimization approach for voltage profile estimation in a radial distribution network with a decreased number of measurements," in *2017 15th International Conference on Electrical Machines, Drives and Power Systems (ELMA)*, June 2017, pp. 26–31.

[25] V. Rigoni and A. Keane, "Remote voltage estimation in lv feeders with local monitoring at transformer level," in *2017 IEEE PES General Meeting*, 2017.

[26] M. E. Baran, J. Zhu, and A. W. Kelley, "Meter placement for real-time monitoring of distribution feeders," in *Proceedings of Power Industry Computer Applications Conference*, May 1995, pp. 228–233.

[27] A. Shafiu, N. Jenkins, and G. Strbac, "Measurement location for state estimation of distribution networks with generation," *IEE Proceedings - Generation, Transmission and Distribution*, vol. 152, no. 2, pp. 240–246, March 2005.

[28] R. Singh, B. C. Pal, and R. B. Vinter, "Measurement placement in distribution system state estimation," *IEEE Transactions on Power Systems*, vol. 24, no. 2, pp. 668–675, May 2009.

[29] K. A. Clements, "The impact of pseudo-measurements on state estimator accuracy," in *2011 IEEE Power and Energy Society General Meeting*, July 2011, pp. 1–4.

[30] E. Manitsas, R. Singh, B. C. Pal, and G. Strbac, "Distribution system state estimation using an artificial neural network approach for pseudo measurement modeling," *IEEE Transactions on Power Systems*, vol. 27, no. 4, pp. 1888–1896, Nov 2012.

[31] J. Wu, Y. He, and N. Jenkins, "A robust state estimator for medium voltage distribution networks," *IEEE Transactions on Power Systems*, vol. 28, no. 2, pp. 1008–1016, May 2013.

[32] S. Bhela, V. Kekatos, and S. Veeramachaneni, "Enhancing observability in distribution grids using smart meter data," *IEEE Transactions on Smart Grid*, vol. PP, no. 99, pp. 1–1, 2017.

[33] M. Pertl, K. Heussen, O. Gehrke, and M. Rezkalla, "Voltage estimation in active distribution grids using neural networks," in *2016 IEEE Power and Energy Society General Meeting (PESGM)*, July 2016, pp. 1–5.

[34] H. Jiang and Y. Zhang, "Short-term distribution system state forecast based on optimal synchrophasor sensor placement and extreme learning machine," in *2016 IEEE Power and Energy Society General Meeting (PESGM)*, July 2016, pp. 1–5.

[35] E. J. Candès and B. Recht, "Exact matrix completion via convex optimization," *Foundations of Computational Mathematics*, vol. 9, no. 6, pp. 717–772, Apr 2009. [Online]. Available: https://doi.org/10.1007/s10208-009-9045-5

[36] S. J. Kim and G. B. Giannakis, "Load forecasting via low rank plus sparse matrix factorization," in *2013 Asilomar Conference on Signals, Systems and Computers*, Nov 2013, pp. 1682–1686.

[37] J. A. Bazerque and G. B. Giannakis, "Nonparametric basis pursuit via sparse kernel-based learning: A unifying view with advances in blind methods," *IEEE Signal Processing Magazine*, vol. 30, no. 4, pp. 112–125, July 2013.

[38] C. Klauber and H. Zhu, "Distribution system state estimation using semidefinite programming," in *2015 North American Power Symposium (NAPS)*, Oct 2015, pp. 1–6.

[39] A. Schmitt and B. Lee, "Steady-state inertia estimation using a neural network approach with modal information," in *2017 IEEE Power Energy Society General Meeting*, July 2017, pp. 1–5.

[40] A. R. Messina and V. Vittal, "Extraction of dynamic patterns from wide-area measurements using empirical orthogonal functions," *IEEE Transactions on Power Systems*, vol. 22, no. 2, pp. 682–692, May 2007.

[41] H. Mehrjerdi, S. Lefebvre, M. Saad, and D. Asber, "A decentralized control of partitioned power networks for voltage regulation and prevention against disturbance propagation," *IEEE Transactions on Power Systems*, vol. 28, no. 2, pp. 1461–1469, May 2013.

[42] A. Schmitt, T. Barik, V. Centeno, and K. Jones, "Empirical synchrophasor-based substation topology estimation," in *CIGRE Science and Engineering*, 2018.

[43] T. K. Barik, A. Schmitt, K. D. Jones, and V. Centeno, "Empirical determination of voltage phasor angle deviation threshold for synchrophasor-based substation topology estimation," in *2017 North American Power Symposium (NAPS)*, Sept 2017, pp. 1–5.

[44] "Ieee standard for synchrophasor measurements for power systems," *IEEE Std C37.118.1-2011 (Revision of IEEE Std C37.118-2005)*, pp. 1–61, Dec 2011.

[45] Grid protection alliance. [Online]. Available: https://www.gridprotectionalliance.org/

[46] A. Schmitt, A. Bernstein, and Y. Zhang, "Matrix completion for low observability voltage estimation," in *IEEE Transactions on Smart Grid*, 2018.

[47] Y. Hu, D. Zhang, J. Ye, X. Li, and X. He, "Fast and accurate matrix completion via truncated nuclear norm regularization," *IEEE Transactions on Pattern Analysis and Machine Intelligence*, vol. 35, no. 9, pp. 2117–2130, Sept 2013.

[48] R. H. Keshavan, S. Oh, and A. Montanari, "Matrix completion from a few entries," *CoRR*, vol. abs/0901.3150, 2009. [Online]. Available: http://arxiv.org/abs/0901.3150

[49] D. Gross, "Recovering low-rank matrices from few coefficients in any basis," *CoRR*, vol. abs/0910.1879, 2009. [Online]. Available: http://arxiv.org/abs/0910.1879

[50] B. Eriksson, L. Balzano, and R. D. Nowak, "High-rank matrix completion and subspace clustering with missing data," *CoRR*, vol. abs/1112.5629, 2011. [Online]. Available: http://arxiv.org/abs/1112.5629

[51] E. J. Candes and Y. Plan, "Matrix completion with noise," *Proceedings of the IEEE*, vol. 98, no. 6, pp. 925–936, June 2010.

[52] A. Bernstein, C. Wang, E. Dall'Anese, J.-Y. Le Boudec, and C. Zhao, "Load-flow in multiphase distribution networks: Existence, uniqueness, and linear models," 2017, [Online] Available at: http://arxiv.org/abs/1702.03310.

[53] K. Turitsyn, P. Sulc, S. Backhaus, and M. Chertkov, "Local control of reactive power by distributed photovoltaic generators," in *2010 First IEEE International Conference on Smart Grid Communications*, Oct 2010, pp. 79–84.

[54] A. Bernstein and E. Dall'Anese, "Linear power-flow models in multiphase distribution networks: Preprint," May 2017. [Online]. Available: http://www.osti.gov/scitech/servlets/purl/1361015